

## The Structure and Evolution of a Numerically Simulated High-Precipitation Supercell Thunderstorm

MARK S. KULIE AND YUH-LANG LIN

*Department of Marine, Earth, and Atmospheric Sciences, North Carolina State University, Raleigh, North Carolina*

(Manuscript received 22 October 1996, in final form 26 July 1997)

### ABSTRACT

The structure and evolution of a high-precipitation (HP) supercell thunderstorm is investigated using a three-dimensional, nonhydrostatic, cloud-scale numerical model (TASS). The model is initialized with a sounding taken from a mesoscale modeling study of the environment that produced the 28 November 1988 Raleigh tornadic thunderstorm. TASS produces a long-lived convective system that compares favorably with the observed Raleigh tornadic thunderstorm. The simulated storm evolves from a multicell-type storm to a multiple-updraft supercell storm. The storm complex resembles a hybrid multicell-supercell thunderstorm and is consistent with the conceptual model of cool season strong dynamic HP supercells that are characterized by shallow mesocyclones. The origin of rotation in this type of storm is often in the lowest levels.

Interactions between various cells in the simulated convective system are responsible for the transition to a supercellular structure. An intense low-level updraft core forms on the southwest flank of the simulated storm and moves over a region that is rich in vertical vorticity. The stretching of this preexisting vertical vorticity in the storm's lowest levels is the most important vertical vorticity production mechanism during the initial stages of the main updraft's development. Interactions with an extensive cold pool created by the storm complex are also important in producing vertical vorticity as the main updraft grows. Overall, the development of vorticity associated with the main updraft appears similar to nonsupercellular tornadic storms. However, classic supercell signatures are seen early in the simulation associated with other updrafts (e.g., formation of vortex couplet due to tilting of ambient horizontal vorticity, storm splitting, etc.) and are deemed important.

In the storm's supercell stage, rotation is sustained in the lowest levels of the storm despite large amounts of precipitation located near and within the main mesocyclone. Pulsating downdrafts periodically invigorate the storm and the gust front never occludes, thus allowing the main updraft to persist for a prolonged period of time. The storm's intensity is also maintained by frequent updraft mergers.

### 1. Introduction

At about 0600 UTC on 28 November 1988, a powerful (F4), long-lived tornado ravaged portions of north-central North Carolina, including the city of Raleigh. The parent thunderstorm also spawned two weaker tornadoes in extreme northern North Carolina and southeast Virginia later in the morning (Fig. 1). Four lives were lost, 157 people were injured, and total damages exceeded \$77 million (NOAA 1988). The longevity and violence of this event were surprising, as it was a climatologically rare occurrence, forming early in the morning late in the year, and the environment was seemingly not conducive to the formation of severe, convective storms. However, conditions near Raleigh changed very rapidly in the hours before 0600 UTC. The complex evolution of the environment in which this thunderstorm formed has been extensively analyzed in

previous studies (e.g., Browning et al. 1989; Gonski et al. 1989; Mogil and Ellrod 1989; Korotky 1990; Funk 1991; Zack et al. 1993, 1994; Kaplan et al. 1995).

The structure of the Raleigh tornadic thunderstorm was also very intriguing. Przybylinski (1989; hereafter P89) investigated the thunderstorm from a radar perspective and found that it was not a classic supercell storm, but rather a modified supercell whose mesocyclone and tornado were largely embedded in precipitation. These features have been observed in so-called high-precipitation (HP) supercells (Moller et al. 1994). Distinctive kidney or S-shaped echo patterns, inflow notches, and persistent weak echo regions (WERs) are observed in many HP storms, although the radar reflectivity patterns associated with HP supercells are quite diverse (Przybylinski 1993a). Multiple reflectivity cores may also be apparent in some HP storms, as was observed in the Raleigh tornadic thunderstorm. Thus, many hybrid multicell-supercell events (e.g., Foote and Frank 1983; Nelson 1987) may be simply considered one form of the HP supercell. Hook echoes, if present, are often very broad, and many HPs undergo a life cycle in which they evolve from one form to another, with

---

*Corresponding author address:* Dr. Yuh-Lang Lin, Dept. of Marine, Earth, and Atmospheric Sciences, North Carolina State University, Raleigh, NC 27695-8208.  
E-mail: yllin@ncsu.edu

### NORTH CAROLINA-VIRGINIA TORNADES on November 28, 1988

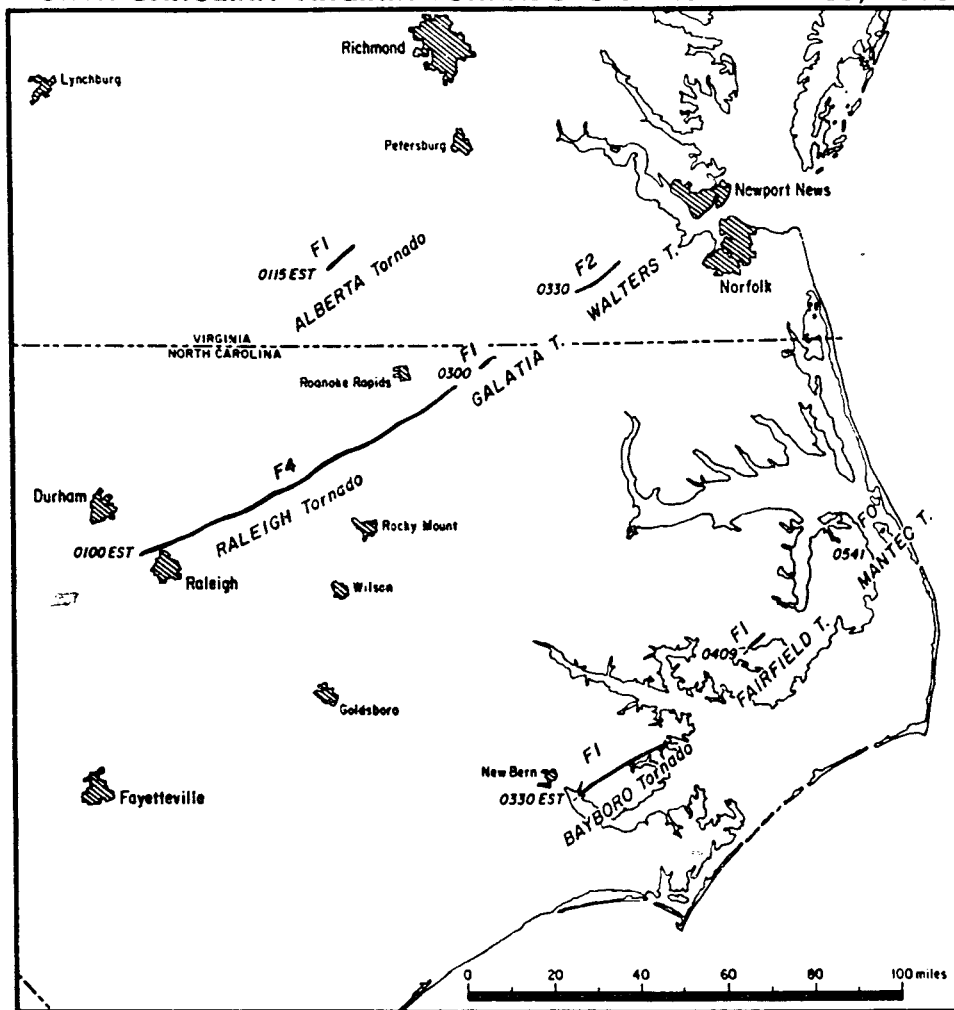


FIG. 1. Damage paths of the tornadoes on 28 November 1988 (from NOAA 1988).

the transition from classic to HP, or HP to bow echo being somewhat common (Przybylinski 1993a). The classic supercell may evolve into an HP-like storm as it decays, but the HP supercell distinguishes itself from the dissipating classic supercell by sustaining its rotation even though its mesocyclone is mired in precipitation. The updraft in some HP supercells is located on the forward flank of the storm, appearing as a rotating comma-shaped structure on the radar, which is often associated with violent tornadoes (e.g., Przybylinski 1989, 1990, 1993a). Some HP storms, like the Raleigh tornadic thunderstorm, occur in a strong dynamic, cool season environment. Doppler radar studies have suggested that HP supercells forming in such an environment often have a shallow mesocyclone depth, and rotation may originate in the storm's lowest levels (Przybylinski 1993b).

Numerical simulations by Brooks et al. (1994) reveal the importance of midlevel (3–7 km) storm-relative

winds in creating some HP-type storms. If the mid-tropospheric storm-relative winds are weaker, precipitation does not fall downwind of the updraft, and the mesocyclone is located in the heavy precipitation. The baroclinic generation of vorticity at low levels is enhanced in this case, and a low-level mesocyclone is quickly created. Because of the strength of the outflow, this mesocyclone is short lived, as the outflow cuts off the main updraft's inflow very quickly. These results offer a reason why HP supercells do not usually produce long-lived tornadoes. Therefore, "external" influences seem to be more important for some HP storms, especially those that produce long tornado tracks (Doswell et al. 1990). This hypothesis seems valid, as HP supercells often move along preexisting baroclinic zones, as in the case of the Raleigh tornado.

Recent research has shown that "nonclassical" supercell storms embedded within larger multicellular convective systems, like the Raleigh tornadic thunder-

storm, account for many significant tornadic events (Johns et al. 1993). However, much of our knowledge of tornadic thunderstorms results from observations of isolated, classic Great Plains supercells. The defining feature of the classic supercell is a persistent, significantly deep, rotating updraft, or mesocyclone. Several other distinguishing structural characteristics are associated with this type of supercell storm, including a main updraft, forward-flank downdraft (FFD), rear-flank downdraft (RFD), hook echo radar signature, flanking line, and bounded weak echo region (BWER) (Lemon and Doswell 1979). Cloud-scale numerical models have successfully produced these attributes, thus allowing investigators to further probe dynamical aspects of this type of convective storm (e.g., Klemp and Wilhelmson 1978; Klemp et al. 1981; Rotunno and Klemp 1985). Numerical models, with further validation of Doppler radar observations (e.g., Johnson et al. 1987) and theoretical work (e.g., Klemp and Rotunno 1983; Davies-Jones 1984; Rotunno and Klemp 1985), have clarified the origin of rotation in classic supercells. First, a midlevel mesocyclone forms due to the tilting of horizontal vorticity created by the ambient vertical wind shear by updrafts. After the midlevel mesocyclone is established, some classic supercells develop rotation in the lowest levels of the storm due to baroclinically produced vorticity along the storm's intense outflow (Rotunno and Klemp 1985; Wicker and Wilhelmson 1995). This horizontal vorticity produced along the gust front of the storm often has a significant streamwise component and is tilted and stretched as it is ingested by the main updraft. This mechanism may also be important in thunderstorms that interact with preexisting baroclinic zones (e.g., thunderstorm outflows) and intensify rapidly, develop rotation, and produce tornadoes (Maddox et al. 1980; Weaver and Nelson 1982; Purdom 1993). It should also be noted that a midlevel mesocyclone is *not* a necessary condition for tornadogenesis (e.g., Carbone 1983; Wakimoto and Wilson 1989; Brady and Szoke 1989). The stretching of low-level preexisting vertical vorticity by rapidly developing updrafts is thought to be responsible for such "nonsupercell" tornadogenesis. Tornadoes under these circumstances are generally weak and short lived, but a few notable exceptions have been documented (e.g., Roberts and Wilson 1995; Wakimoto and Atkins 1996).

Classic supercells have been exhaustively studied because of their readily identifiable features, and they occur in many major tornado outbreaks (Moller et al. 1994). As stated earlier, though, tornadoes are not spawned exclusively by isolated, classic supercells. In addition, it has been recognized that a spectrum of supercell storms exists consisting of variations from the classic supercell model (Moller et al. 1994), such as "low-precipitation" (e.g., Bluestein and Parks 1983) and HP supercells. The definition of a supercell becomes clouded in light of all the forms it may take. To ease confusion, a supercell will be defined as a thunderstorm

that has a persistent mesocyclonic circulation throughout a significant portion of the storm.

This paper presents results from a cloud-scale numerical simulation of a multiple updraft HP storm complex (a nonclassical supercell event), with the Raleigh tornadic thunderstorm serving as the motivation for undertaking this study. The model is initialized with a vertical profile taken from a coupled mesoscale–cloud-scale modeling study of the Raleigh tornadic thunderstorm (Zack et al. 1994; hereafter Z94). Z94 focused on the *general* features of the convection produced by the cloud model and did not provide a detailed examination of the evolution and structure of the simulated thunderstorms. Our efforts are aimed at exclusively studying the details of the storm generated by the 0600 UTC Raleigh sounding from Z94's mesoscale simulation. Thus, the horizontal and vertical grid resolutions are finer than those used by Z94's cloud-scale study, and the present simulation is integrated for a longer duration to better investigate the modeled storm. The lack of modeling studies on HP and other nonclassical supercells, especially since these storms frequently produce damaging wind, torrential rain, large hail, and tornadoes in the southeast United States, provides further motivation for this study.

By examining the structure and evolution of the simulated storm, we attempt to answer the following questions: 1) Can a numerical model capture the general characteristics of the convection that occurred on 28 November 1988? 2) What mechanisms are responsible for the longevity of certain HP supercells that produce long-lasting low-level mesocyclones? 3) Are there any special dynamical aspects of certain nonclassical supercell thunderstorms that differentiate them from classic supercells? It is not our intention to reproduce the *exact* storm observed on 28 November 1988 but to concentrate on certain basic features of the convection that can be generated in such an environment and to compare the results against various conceptual models of supercells. To evaluate the numerical model's ability to produce a *similar* convective storm, comparisons will be made to the actual Raleigh tornadic thunderstorm.

Section 2 describes the numerical model employed and initialization procedures, and section 3 presents general results of the simulation. The updraft structure and intensification mechanisms are discussed in section 4. Section 5 explores the growth of vorticity in the simulation. A summary and conclusions are presented in section 6.

## 2. Numerical model description and initialization

The Terminal Area Simulation System (TASS) is used to study the cloud-scale features and evolution of the thunderstorm responsible for producing the 1988 Raleigh tornado. TASS is a time-dependent, three-dimensional, nonhydrostatic cloud model that has successfully simulated many different forms of convection and has

been used extensively in analyzing microburst-producing thunderstorms (Proctor 1989, 1992). The model contains prognostic equations for momentum, pressure deviation, potential temperature, and the continuity of various water substances including water vapor, cloud droplets, rain, snow, and hail. TASS incorporates the Adams–Bashforth time-differencing scheme, whereas a second-order quadratic-conservative method is used for space differencing. The Orlanski (1976) radiation boundary condition is applied to open lateral boundaries, while a filter and sponge are applied to the top four grid points. Subgrid processes are parameterized by the Smagorinsky (1963) subgrid-turbulence closure scheme with Richardson number dependence, and a surface friction layer is included using Monin–Obukhov (1954) similarity theory. TASS contains complete liquid and ice-phase microphysical parameterizations, similar to Lin et al. (1983). The model also features vertical grid stretching, as well as a grid mesh that translates with the simulated convection, thus eliminating the need for a large horizontal domain. A detailed model description is presented in Proctor (1987, 1996).

The total horizontal domain used in this simulation is  $54 \text{ km} \times 54 \text{ km}$ , and the vertical domain extends to 20 km. The horizontal grid spacing is a uniform 750 m, and the vertical grid spacing stretches from 100 m near the surface to 700 m near the domain top (50 levels). A thermal perturbation ( $3.5^\circ\text{C}$ ) with a horizontal (vertical) radius of 10 km (1.5 km) is applied to the horizontally homogeneous basic state to induce convection. The total simulation time is 240 min. The model time step varies and is automatically calculated by TASS to assure numerical stability.

TASS is initialized using a single sounding generated by the Mesoscale Atmospheric Simulation System (MASS)—a mesoscale numerical model (MESO 1993). The MASS sounding (Fig. 2) was extracted at a grid point near Raleigh at 0600 UTC in simulated time (Z94). The wind profile and convective available potential energy (CAPE) of the MASS sounding compare favorably with a proximity sounding created for the actual environment that produced the Raleigh tornadic thunderstorm (Gonski et al. 1989). The CAPE ( $\sim 1200 \text{ J kg}^{-1}$ ) associated with this sounding is considered marginal for the development of severe convection. The environmental wind shear is rather strong, though, producing a bulk Richardson number (BRN) of 7. Supercells primarily occur in environments characterized by BRN values between 10 and 40 (Weisman and Klemp 1984). A BRN of less than 10 is thought to possess shear that is too strong for even supercell development, but many cold season, strong dynamic events fit into this category (Johns et al. 1993). The 0–6-km mean wind is about  $30 \text{ m s}^{-1}$  from  $222^\circ$ . The 3–7-km storm-relative wind shear is only  $\sim 0.003 \text{ s}^{-1}$ , and precipitation in the simulated storm is anticipated to be located close to the updrafts (Brooks et al. 1994). Using an average storm speed and motion from the simulated storm of 22

$\text{m s}^{-1}$  from  $226^\circ$ , the storm-relative helicity for this model sounding is about  $400 \text{ m}^2 \text{ s}^{-2}$  indicating the potential for supercells capable of producing strong tornadoes (Davies-Jones et al. 1990).

### 3. Results

TASS produces an intense, long-lived convective system that evolves from a multiple-updraft storm to a HP supercell with significant storm-scale rotation. This section presents the results of the simulation, with individual subsections that focus on the general features of the convection, a comparison of the simulated storm to observations of the actual Raleigh tornadic thunderstorm, and the simulated storm's structural evolution.

#### a. General results

The domain maximum values of vertical velocity and vertical vorticity, as well as minimum values of vertical velocity, are depicted in Fig. 3. After displaying roughly cyclic features in the first hour of the simulation as the convection organizes, the maximum vertical velocity and vorticity fields appear quasi-steady between about 60 and 105 min. Between 120 and 180 min, the maximum updraft velocity oscillates between  $23 \text{ m s}^{-1}$  and  $30 \text{ m s}^{-1}$ , whereas the maximum downdraft velocity strengthens to about  $-17 \text{ m s}^{-1}$ . An abrupt increase in vertical vorticity ( $\sim 0.05 \text{ s}^{-1}$ ) is also observed during this time, indicating strong rotation within the storm. Maximum values of vertical velocity gradually decline between 180 and 210 min, but the updraft strengthens again by 225 min. The maximum downdraft follows the same general pattern as the positive vertical motions, as it weakens after about 170 min, but then increases in magnitude after 225 min. The maximum vertical vorticity never attains values greater than  $0.035 \text{ s}^{-1}$  for the last 75 min of the simulation, although values greater than  $0.025 \text{ s}^{-1}$  are sustained throughout this time.

Figure 4 shows the radar reflectivity at low and middle levels between 60 and 180 min. The general echo structure is elongated and oriented from southwest to northeast from 60 to 120 min. Multiple reflectivity cores are evident, and the areal extent of the echo mass grows substantially throughout this time. By 90 min, a narrow swath of heavy precipitation forms within the larger area of precipitation. Tight reflectivity gradients are located on the right flank of the storm, and numerous reflectivity notches develop in regions of storm inflow. The multicellular nature of the system is also evident in the  $z = 5 \text{ km}$  reflectivity field shown in Fig. 4 (dashed line). New reflectivity cores are generated along the southwest side of the line, as is often observed in multicells. The cells and the echo mass move northeastward in the direction of the 0–6-km mean wind.

The radar reflectivity has a rather steady appearance from 120 to 150 min. The structure is elongated with a broad pendant extending to the southwest, and the re-

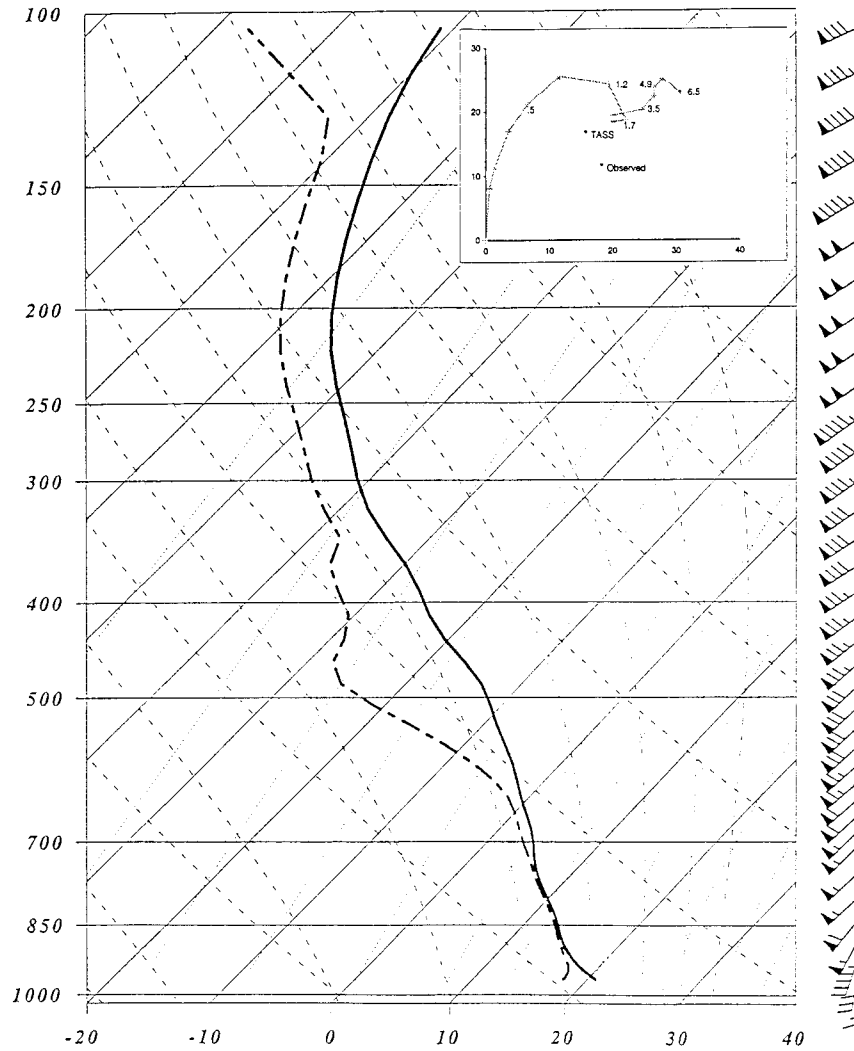


FIG. 2. The MASS sounding and associated hodograph used for model initialization. Temperature (solid) and dewpoint temperature (dashed) in degrees Celsius, as well as the wind profile, are shown.

flectivity gradient is very tight on the right flank. The maximum reflectivity gradually shifts to the southwest throughout this time period. Numerous cores of heavy precipitation form after 140 min in response to both the rapid strengthening of a major updraft and the merger of smaller cells within the storm complex. An extensive WER develops on the storm's right flank, as shown by the overhang in the  $z = 5$  km reflectivity fields. This large WER is a manifestation of the strong updrafts associated with the convective system.

The radar reflectivity displayed in Fig. 4 slowly evolves after  $\sim 155$  min as the storm becomes more supercellular in appearance. A narrow band of heavy precipitation still exists at 165 and 175 min, but it is tilted more in the north-south direction due to the intense inflow and storm-scale rotation that develops. A 60-dBZ core forms at 165 min at 410 m (Fig. 4h), as well as a broad hook echo. By 180 min, the hook

echo evolves into a pendant echo that trails to the south (Fig. 4i). A new line of precipitation forms behind the main updraft. The two echo cores are separated by a weak reflectivity notch (WRN) that appears at 165 min.

Figure 5 shows time-height cross sections of domain maximum vertical velocity, vertical vorticity, and radar reflectivity. The maximum vertical velocity is largely confined to upper levels ( $>8$  km) of the convective system in the first half of the simulation (Fig. 5a). Significant values of vertical vorticity ( $>0.01 \text{ s}^{-1}$ ) are evident during this time, but closer examination of the model output reveals that they are not highly correlated with any updrafts in the storm's upper levels (Fig. 5b). However, significant vertical vorticity is present in the lowest 2 km after about 75 min and persists through the remainder of the simulation. After 120 min, the cyclic production of upper-level updraft maxima continues.

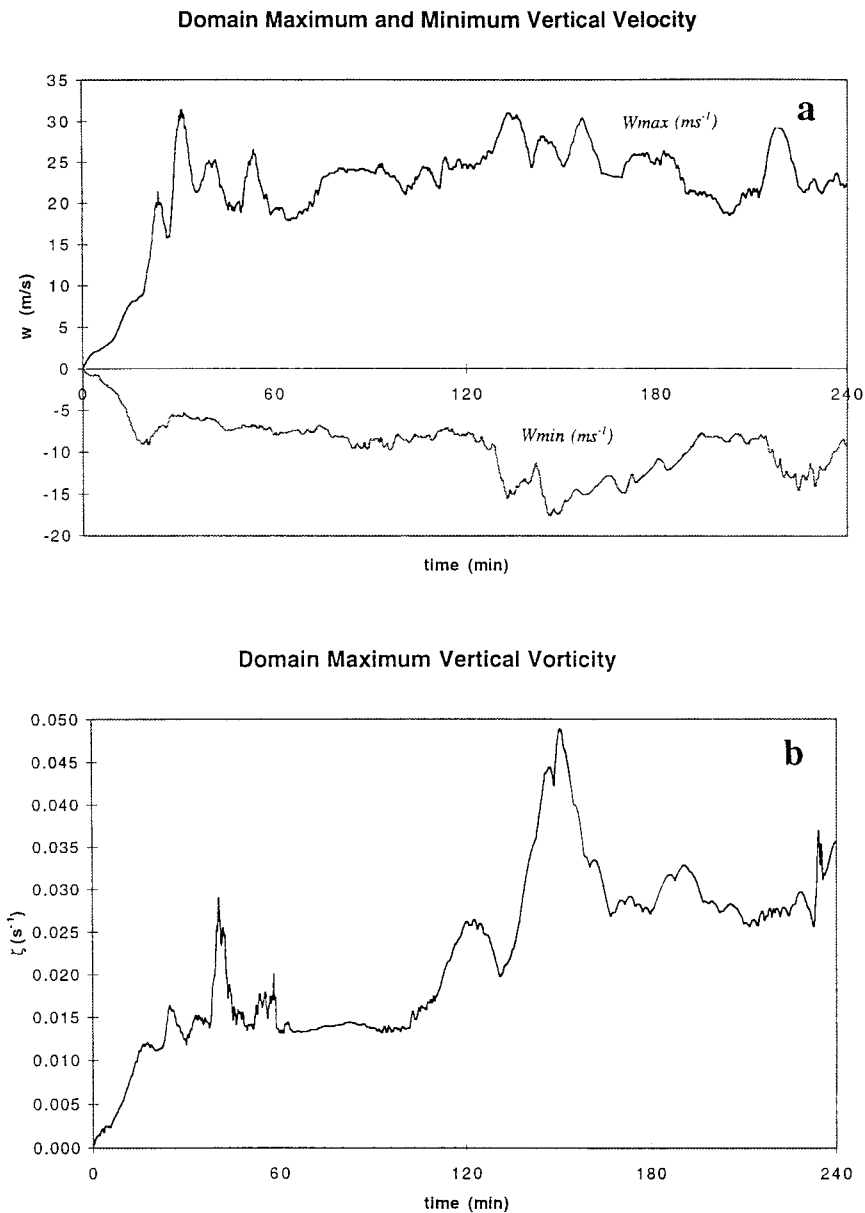


FIG. 3. (a) Domain maximum vertical velocity and minimum vertical velocity, and (b) domain maximum vertical vorticity.

Three major low-level updraft cores, though, form between 120 and 240 min. The updraft maxima at 165 min centered at about  $z = 3$  km is especially impressive (Fig. 5a) and coincides with large values of vertical vorticity below 3 km (Fig. 5b). These figures suggest that the simulated storm undergoes a transition in which it acquires intense low-level rotation. This transition, as well as the development of vorticity, will be discussed further in later sections.

Overall, Figs. 3, 4, and 5 reveal an intense, long-lived convective storm with considerable rotation. The storm can rarely be described as “steady,” however, as os-

cillations appear in many fields throughout the simulation. Figures 3 and 5 nicely illustrate some general characteristics of the simulated storm, although they should be analyzed with caution. The simulation produces a multiple-updraft system, and the domain maximum values are sometimes located in different cells, especially before about 120 min. After this time, one updraft becomes dominant, and the domain maximum values can be attributed to this cell. The development of this intense cell, as well as the overall structure of the evolving storm, will be analyzed further in the following sections.

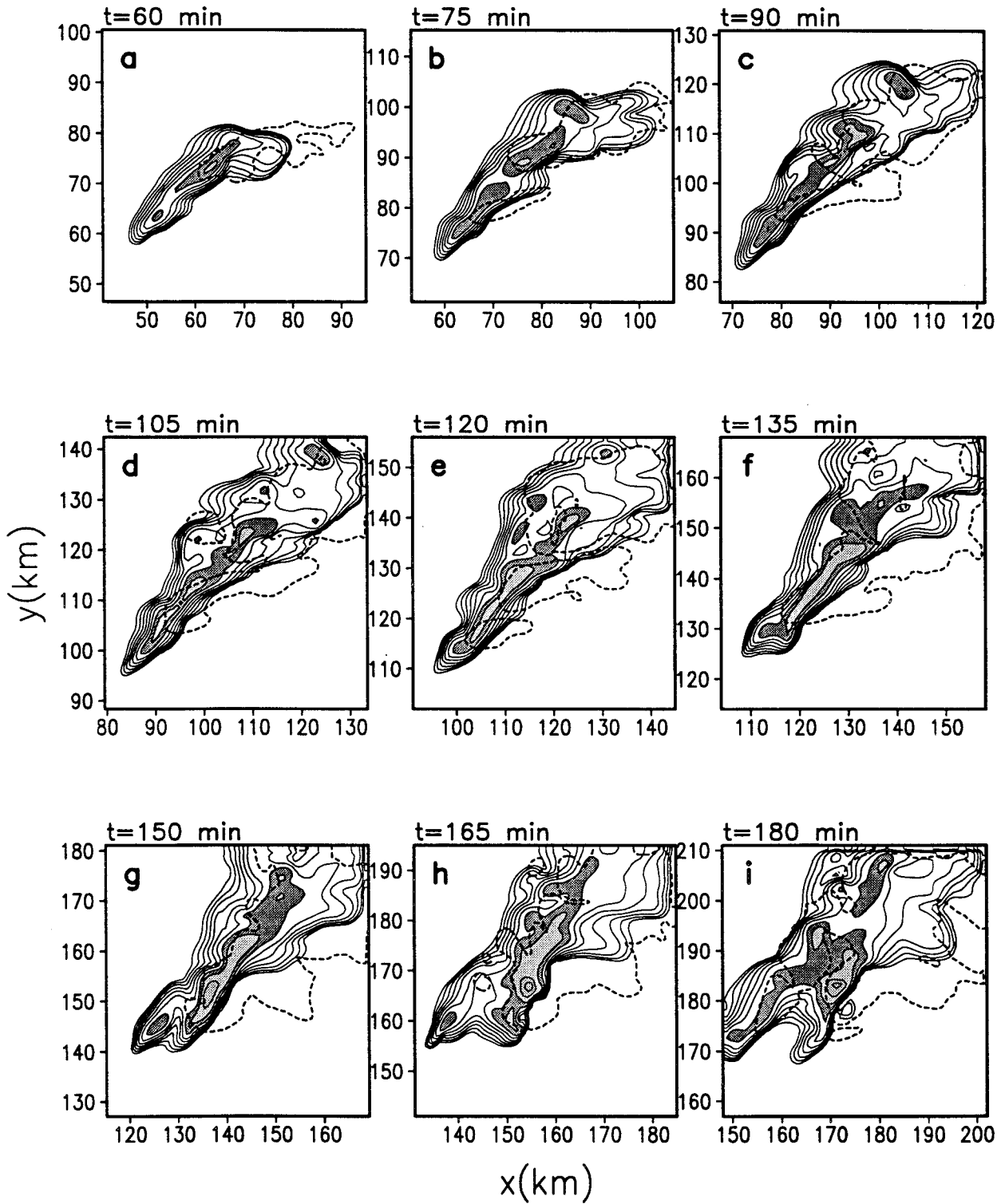


FIG. 4. Radar reflectivity at  $z = 410$  m and 4.9 km from 60 to 180 min at 15-min intervals. Solid contours are the radar reflectivity at  $z = 410$  m in 5-dBZ intervals. The minimum contour is 15 dBZ. Shaded areas indicate radar reflectivity cores of greater than 45, 50, and 55 dBZ, respectively. The dashed line is the 25-dBZ contour at  $z = 4.9$  km.

### b. Comparison to the Raleigh tornadic thunderstorm

Table 1 compares various characteristics of the observed Raleigh tornadic thunderstorm to the simulated storm. While the average storm speed of the simulated storm is comparable, a small discrepancy exists in the storm motion. The actual thunderstorm was influenced by a preexisting mesoscale boundary and other scale-interactive features. TASS cannot adequately account for these features in its horizontally homogeneous initial state, and the simulated storm motion may subsequently be affected. During the last 30 min of the simulation, the simulated storm moves from  $\sim 233^\circ$ , which is in closer agreement to the observed thunderstorm motion of  $\sim 240^\circ$ . The other features of the simulated thunderstorm shown in Table 1 compare very favorably with the observed storm.

Many of the radar features produced by TASS are strikingly similar to the observed radar signatures of the Raleigh tornadic thunderstorm. Figure 6 is taken from P89's radar study of the Raleigh thunderstorm. The orientation and structure of the radar echoes compare favorably to those in Fig. 4. Multiple high reflectivity cores are observed in both figures, with the third mesocyclone (M3) and reflectivity core (R3) in Fig. 6 producing the Raleigh tornado. The simulated storm follows the same progression, as the third major updraft in the storm's multicell stage acquires the most intense rotation. Also, the production of significant updrafts on the southwest flank of the actual storm ceases after M3 forms. A flanking line exists, but no major updrafts are forced between 0608 and 0647 UTC directly behind M3. Similar qualities exist in the simulation, as there is no significant updraft production on the southwest flank of the major updraft after  $\sim 155$  min, and a weak flanking line forms. Last, the development of WRNs behind the main updraft occurs in both the actual and simulated storms. P89 hypothesizes that the WRNs in the actual storm result from a pulsating RFD that continually invigorates the thunderstorm. As will be shown in a later section, a pulsating RFD is observed in the simulation. Overall, TASS adequately captures the general characteristics of the convection that occurred on 28 November 1988.

### c. Storm structure and evolution

The following four sections concentrate on the structure and evolution of the simulated storm. Four stages of the modeled thunderstorm are observed: 1) the multicell stage (0–120 min), 2) the transition stage (120–155 min), 3) the supercell stage (155–210 min), and 4) the reintensification stage (210–240 min).

#### 1) THE MULTICELL STAGE (0–120 MIN)

The simulated storm displays mostly multicellular characteristics throughout the first 120 min. Numerous

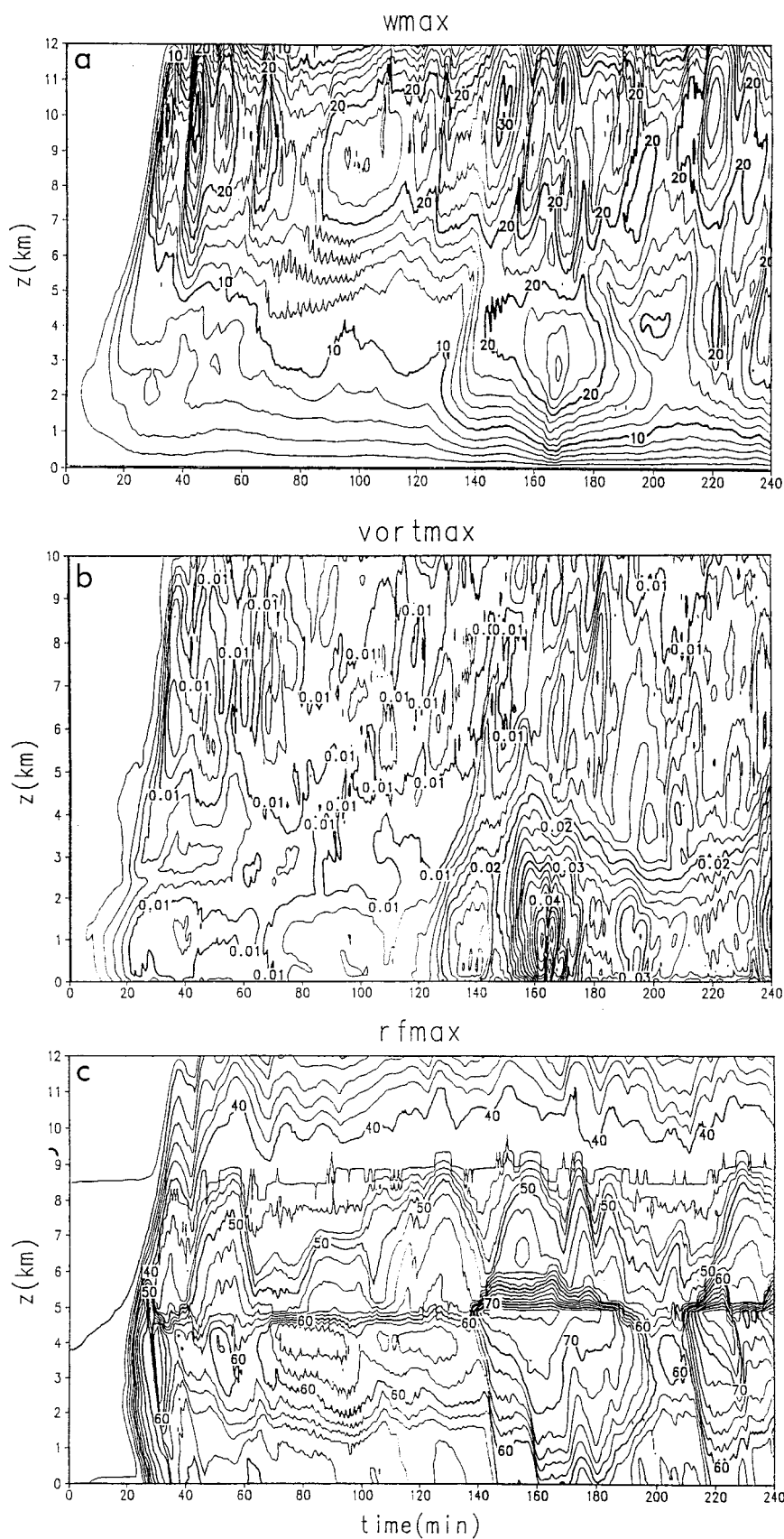
cells develop and dissipate throughout this time in a fairly unorganized fashion. Four dominant cells, however, are organized and have lifetimes exceeding 1 h. These cells are largely responsible for the structure of the simulated storm and play important roles in the subsequent transition to the supercell stage. Even though the simulated storm does not conform *exactly* to classic multicell conceptual models, the continual formation of updrafts on the southwest flank of the convective system is the defining feature of this stage that are consistent with typical multicells (e.g., Marwitz 1972). The ending time of 120 min for the multicell stage is rather arbitrary, as multiple updrafts are observed throughout most of the simulation. Other structural changes in the simulated storm are apparent after 120 min, thus providing a convenient cutoff for this particular stage.

Figure 7 depicts areas of positive vertical motion and the storm-relative horizontal velocity vectors at  $z = 2.1$  km. At 80 min (Fig. 7a), three main updrafts are present, with a fourth updraft, U4, just forming on the rear flank of the storm complex. In general, the cells on the northeast section of the system are oldest and weaken over time. The main updraft cores are embedded within a broad updraft region, similar to observations of transitory and hybrid multicell-supercell storms (e.g., Foote and Frank 1983; Vasiloff et al. 1986; Nelson 1987). This feature is not fully captured in Fig. 7 because the zero contour is suppressed. These updrafts are all associated with vertical vorticity at  $z = 2.1$  km of up to  $0.008 \text{ s}^{-1}$  (Fig. 8b), suggesting developing rotation within the updrafts. Interestingly, U1 is the only updraft showing intense rotation during the multicell stage, albeit *anticyclonic* rotation. This updraft moves quickly out of the domain and appears to be a typical left-moving storm that arises from the storm-splitting process observed in classic supercells (e.g., Klemp 1987).

Figures 8a and 8c show that the vertical vorticity in the lowest levels is significant in the vicinity of U3 and U4 from 80 to 120 min. This axis of maximum low-level vorticity exceeding  $0.012 \text{ s}^{-1}$  occurs along the southwest section of an extensive ( $\sim 50$  km long), shallow ( $< 1$  km deep) cold pool (Fig. 9a). A continuous updraft forms along this boundary and is most intense under U3 and U4. The storm-relative wind flow is from the southeast to the right of the cold pool. The winds then turn cyclonically around the zone of convergence at the head of the gust front. An axis of maximum storm-relative winds also forms immediately behind the leading edge of the cold pool. As will be seen, this feature is important in the transition of the storm to a more supercellular form.

#### 2) THE TRANSITION STAGE (120–155 MIN)

This time period is characterized by the explosive intensification of U4. While multiple updrafts still exist, the multicellular structure of the storm becomes less obvious, and U4 becomes the dominant feature by 155



min. A rapid increase in vertical vorticity also occurs, and a well-defined mesocyclone develops in the lowest portions of the storm. As stated earlier, the exact times of the various stages of the simulated storm are not well defined. The transition process may actually commence at an earlier time when U4 first begins to strengthen. However, an increase in speed of U4, as well as the acquisition of rotation and formation of extensive downdrafts, are features that appear between 120 and 155 min that define this particular stage.

Cell U4 undergoes a pronounced transformation during the transition stage. Its updraft intensity at  $z = 2.1$  km increases from  $\sim 8 \text{ m s}^{-1}$  at 120 min to greater than  $19 \text{ m s}^{-1}$  by 155 min. It also moves much faster to the northeast ( $\sim 26 \text{ m s}^{-1}$ ) than the previous stage. Figure 10 shows regions of positive vertical motion and storm-relative wind vectors at  $z = 2.1$  km at 130 and 155 min. The increase in U4's strength, as well as the decrease in distance between U3 and U4, are obvious structural changes in the storm. New updraft perturbations form ahead of U4 at 155 min and are part of a broad sustained region of vertical motion in the storm complex. The storm-relative horizontal wind field at  $z = 2.1$  km is dominated by the continued cyclonic curvature about the broad updraft region early in the transition stage (Fig. 10a). By 155 min, though, a well-defined circulation about 5 km wide develops that is coincident with U4 (Fig. 10b). An increase in vertical vorticity at  $z = 710$  m from  $0.018$  to  $0.023 \text{ s}^{-1}$  occurs accordingly with the development of rotation (Figs. 11a and 11c). At  $z = 2.1$  km, the vertical vorticity increases from  $0.016$  to  $0.025 \text{ s}^{-1}$  (Figs. 11b and 11d). Significant vertical vorticity extends from 0 to 3 km at 130 min, with the most intense values initially located under 1 km. *This fact suggests that the rotation in U4 originates from the lowest portions of the storm.* The development of vorticity in U4 will be discussed in greater detail in a later section.

Significant low-level features at 155 min are shown in Fig. 9b. There is a marked increase in the strength of low-level inflow at 155 min, and increased convergence along the cold pool intensifies the updraft at  $z = 410$  m considerably. The cold pool continues to expand and strengthen. A noticeable bulge and strong gradient appears in the perturbation temperature field at 155 min.

A last defining structural feature of the transition stage is the formation of an extensive downdraft on the left flank of the updrafts. This long ( $>20$  km), narrow downdraft at 140 and 145 min is shown in Fig. 12. Two downdraft cores exist beside U3 and U4, respectively. The broad downdraft coincides with the heaviest core of precipitation, indicating that precipitation effects may be primarily responsible for the downdraft's existence.

Such downdrafts have been proposed to play a vital role in the formation and maintenance of severe hybrid multicell-supercell hailstorms by promoting stronger convergence and updrafts along the gust front (Nelson 1987).

### 3) THE SUPERCELL STAGE (155–210 MIN)

From 155 to 210 min, U4 is the dominant feature of the storm complex. A mesocyclone develops and persists throughout this time period. The appearance of the updraft is much steadier than previous stages, as the main updraft maintains a compact, comma-shaped appearance from 155 to 185 min and is intensely rotating (Fig. 13a). After this time, U4 expands into a configuration similar to the elongated updraft structure during the transition phase, but still retains weaker rotation (Fig. 13b).

Figure 14a is a detailed depiction of U4 at  $z = 1.5$  km at 155 min. The reflectivity field is a pronounced "S" shape and heavy precipitation is located close to and within the mesocyclone—both characteristics of HP supercells. The storm-relative wind field reveals an almost closed circulation coincident with the main updraft, and the mesocyclone's vertical extent is significantly deep ( $\sim 5$  km). By 165 min, a pronounced hook echo wraps around U4 (Fig. 14b). An extensive downdraft exists on the left rear flank of U4. At  $z = 1.1$  km, an intense core ( $\sim -5 \text{ m s}^{-1}$ ) within this downdraft is located directly to the southwest of U4 (Fig. 15a). This downdraft originates between 2 and 3 km and is analogous to the RFD in a classic supercell. The formation of the RFD is due mostly to dynamical effects, as it is found within a region of dynamically induced downward directed perturbation pressure gradients. However, the rear downdraft also coincides with the heavy core of precipitation to the left and rear of U4. Thus, it appears that the downdraft arises from both dynamical and precipitation effects. The RFD is well defined from 155 to 160 min, but then weakens considerably between 160 and 170 min. At 175 min, it intensifies again (Fig. 15c). At 175 min, there are actually two downdrafts on the west and southwest flank of U4. The second core (C2) is not associated with heavy precipitation, but is part of a pronounced inflow region into the rear of the storm originating above 2 km, similar to the RFD that periodically wraps around the main updraft. After 185 min, C2 lags behind U4, and the rear inflow decreases in magnitude.

The structure of the storm noticeably changes from 155 to 165 min as U4 reaches its most intense stage. At 165 min, a forward-flank downdraft (FFD) develops ahead of U4 (Fig. 15b). The emergence of this down-

←

FIG. 5. Time–height cross sections of domain maximum (a) vertical velocity, (b) vertical vorticity, and (c) radar reflectivity. The contour intervals are (a)  $2 \text{ m s}^{-1}$ , (b)  $0.002 \text{ s}^{-1}$ , and (c) 2 dBZ.

TABLE 1. Comparison of various features between the simulated and the observed Raleigh tornadic thunderstorm.

	Observed	TASS
Storm speed	≈20–25 m s <sup>-1</sup>	≈21–26 m s <sup>-1</sup>
Storm direction	From 240°	From 226°
Max cloud-top height	≈14 km	≈14 km
Multiple mesocyclones	Yes	Yes
Multiple high reflectivity cores	Yes	Yes
Modified/HP supercell	Yes	Yes
Inflow notches (forward and rear)	Yes	Yes
Max radar reflectivity (≈2 km)	>47 dBZ	≈65 dBZ
Depth of storm inflow	≈2–3 km	1.5–3.5 km
Surface hail	No	No

draft completes the transition of U4 to a supercellular form. Figure 16 shows the low-level gust front structure at 165 min. Ground-relative winds at the surface approach 30 m s<sup>-1</sup> in the storm's inflow region directly southeast of U4. The intense FFD creates strong divergence in the ground-relative wind field at (x, y) ~ (153,167 km) and enhances the temperature gradient

along the preexisting cold pool. The FFD helps to create a 6-km zone of intense convergence and uplift to the northeast of U4 where it collides with the inflow from the south. A distinctive bulge is located to the south of the main updraft due to the strong east-southeastward flow in the rear gust front. The gust front never occludes, however, thus allowing U4 to maintain its structure for

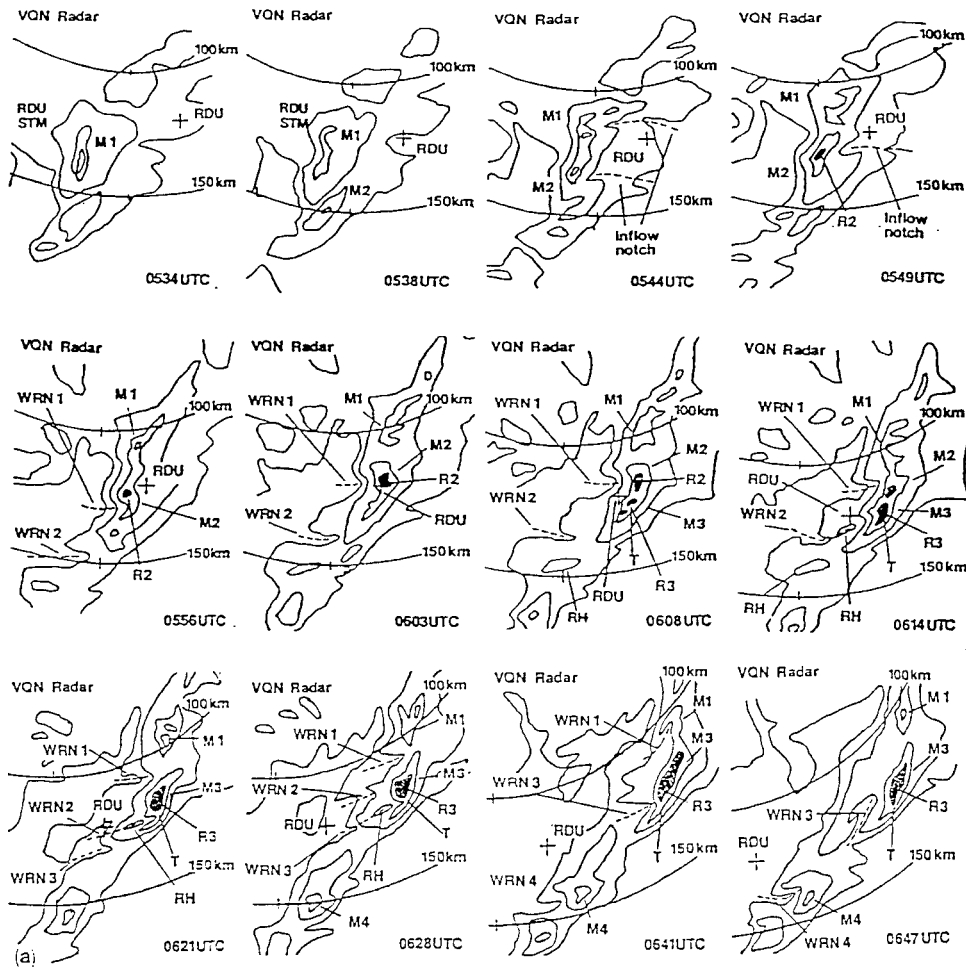


FIG. 6. Evolution of the radar reflectivity for the actual Raleigh tornadic thunderstorm from the Volens, VA, radar site. Contours are given at 18, 30, and 41 dBZ. Shaded regions indicate reflectivity values greater than 47 dBZ. Various mesocyclones are denoted by M, high reflectivity cores by R, weak reflectivity notches by WRN, and reflectivity holes by RH. The location of the tornado is labeled "T" (from P89).

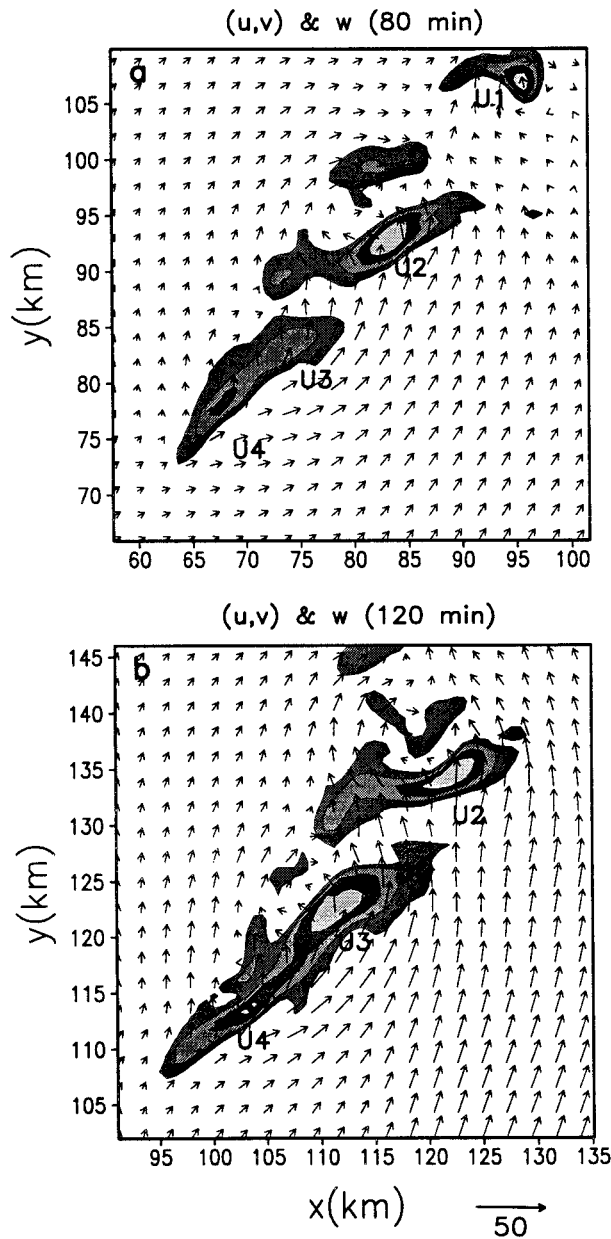


FIG. 7. Storm-relative horizontal wind vectors and upward motion at  $z = 2.1$  km for (a) 80 and (b) 120 min. The contour levels are 2, 4, 6, and  $8 \text{ m s}^{-1}$ . The wind vectors are plotted at every third grid point for clarity. Various updrafts are labeled accordingly.

a long period of time. A possible mechanism that could inhibit the gust front occlusion is the strength of the ambient low-level wind shear, which may be strong enough to combat the surging rear section of the gust front. The balance between the circulation associated with the negative vorticity produced by the cold pool and the positive vorticity of the ambient low-level shear can be written as

$$\left( g d_c \frac{\Delta \theta}{\theta_o} \right)^{1/2} = \Delta \bar{u}|_0^H, \quad (1)$$

where  $d_c$  is the depth of the cold pool,  $\Delta \theta$  the potential temperature deficit of the cold pool,  $\theta_o$  a reference potential temperature,  $H$  the shear depth, and  $\Delta \bar{u}$  the magnitude of the basic-state wind shear up to the level  $H$ . This balance has been shown to be an important factor in the maintenance of certain long-lived convective storms (e.g., Rotunno et al. 1988). Analysis of the low-level shear and horizontal vorticity production about the  $y$  axis at 165 min shows that the low-level shear dominates in the portion of the gust front to the south of U4. The rear section of the gust front is relatively shallow and the temperature deficit is quite weak. Using a cold pool depth of  $\sim 700$  m, a potential temperature deficit of 1.5 K, and a reference temperature of 297 K yields a value of  $\sim 6 \text{ m s}^{-1}$ . Comparatively, the strength of the low-level wind shear in the lowest 1 km of the environment is  $\sim 17 \text{ m s}^{-1}$ . Therefore, the low-level shear is strong enough to prevent the progression of the rear section of the cold pool around the main updraft. Immediately after 165 min, the gust front bulge disappears, and periodic smaller bulges are evident in the next 30 min. The dominance of the shear-induced circulation is also consistent with the structure of the thunderstorm. The main updraft is not erect, but rather tilts to the northeast, as is expected when the low-level shear is very strong and an “optimal” balance between the cold pool and shear does not exist.

A BWER is also present at 165 min, indicating a vigorous updraft (Fig. 17). Intense inflow from the south and east feeds the main cell below 3 km. Weaker inflow occurs between 4 and 6 km. An intense updraft exists with two cores greater than  $25 \text{ m s}^{-1}$ . One updraft core is centered at  $\sim 2.5$  km, while the other is in the upper levels of the storm ( $\sim 9$  km). The emergence of this intense low-level core creates a large  $\partial w / \partial z$ , thus amplifying the vertical vorticity to over  $0.04 \text{ s}^{-1}$  through increased stretching.

The maximum vertical velocity and vorticity at  $z = 2.1$  km, as well as the minimum vertical velocity at  $z = 2.1$  km (associated with the FFD) and the minimum perturbation temperature at the surface, for U4 during the supercell stage are given in Fig. 18. The main updraft speed increases until 167 min when it reaches a peak value of  $23 \text{ m s}^{-1}$  (Fig. 18a). Cell U4 then steadily weakens at  $z = 2.1$  km, falling to  $\sim 11 \text{ m s}^{-1}$  by 210 min. The vertical vorticity follows the same pattern, increasing to  $0.031 \text{ s}^{-1}$  at 165 min, then gradually decreasing afterward (Fig. 18b). Even though the vorticity weakens, a significant value of  $0.021 \text{ s}^{-1}$  exists at 210 min, and strong rotation is evident near  $z = 1.5$  km. The mesocyclone depth decreases to about 3.5 km at 200 min, and the width of the mesocyclone contracts. The strength of the FFD follows this same trend, reaching its strongest point at 162 min and decreasing in intensity afterward (Fig. 18a).

Overall, the simulated storm becomes a self-sustaining system during its supercell stage by producing its own strong microscale baroclinic zone along its forward

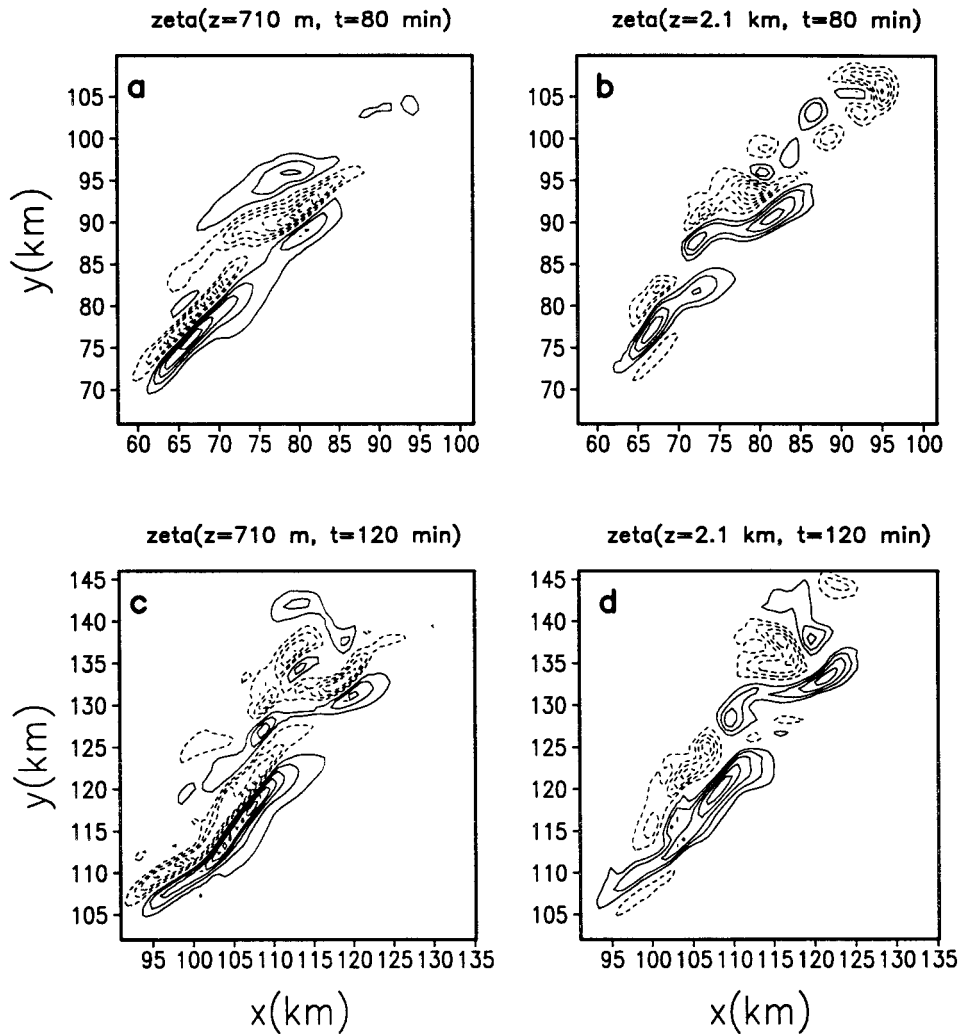


Fig. 8. Vertical vorticity at 80 min for (a)  $z = 710$  m and (b)  $z = 2.1$  km, and vertical vorticity at 120 min for (c)  $z = 710$  m and (d)  $z = 2.1$  km. The contour interval is  $0.002 \text{ s}^{-1}$ . The zero contour is suppressed.

gust front. It does not rely on interactions with other cells in the convective system to generate vorticity and updraft strength, as it did in the transition stage. However, the importance of storm-scale interactions between the various cells during the transition stage cannot be overlooked. Such interactions have been reported as mechanisms for storm intensification and tornadogenesis (e.g., Weaver and Nelson 1982; Purdom 1993). Cell U4 benefits greatly from the cold pool that is generated by cells U2 and U3. The enhanced convergence along this boundary acts to strengthen the updraft and creates a region that is rich in vertical vorticity that U4 moves through. This preexisting vorticity in the vicinity of the cold pool, as well as the baroclinic generation of vorticity along the thermal boundary, is ingested into U4 during its developing stages (before its strong FFD forms), thus helping it evolve into a supercellular structure.

The simulated storm possesses many characteristics

of a mature supercell and is obviously very intense. An intense low-level mesocyclone develops within the mature storm, and rotation is evident near the surface during the storm's most intense stages. The mesocyclone also has a "split" appearance consisting of both updraft and downdraft, and the gust front periodically bulges out. These traits have been observed in actual tornadic thunderstorms (e.g., Lemon and Doswell 1979). Also, recent numerical simulations of tornadic supercells that resolved a tornado vortex have shown that intense updraft pulses extending down to lower levels are associated with the rapid intensification of low-level vorticity that are associated with tornadogenesis (Wicker and Wilhelmson 1995). The TASS simulation produces similar results, as low-level updraft pulses coincide with intense low-level rotation (see Fig. 5). Unfortunately, we can speculate only whether tornadogenesis occurs in the simulation because the horizontal grid resolution is too coarse to resolve an actual tornado vortex. Further

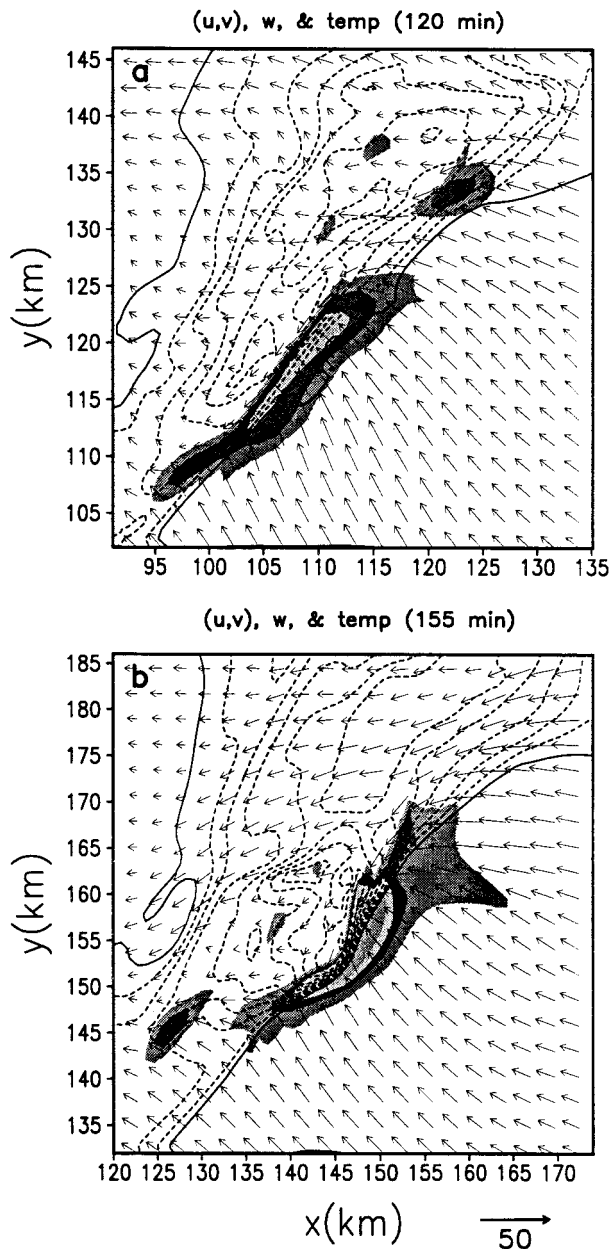


FIG. 9. Storm-relative horizontal wind vectors, negative perturbation temperature (dashed) at  $z = 50$  m, and positive vertical velocity (shaded) at  $z = 410$  m for (a) 120 and (b) 155 min. The contour interval for perturbation temperature is 0.25 K. The solid line denotes the 0-K contour. Positive vertical velocity is shaded at different scales at 1, 2, 3, and 4  $m s^{-1}$ . The wind vectors are plotted at every other grid point.

simulations incorporating a finer grid mesh would provide more insight into the issue of tornadogenesis in such a storm.

4) THE REINTENSIFICATION STAGE (210–240 MIN)

The simulated storm reintensifies over the final 30 min of the simulation. Cell U4 reaches its weakest point

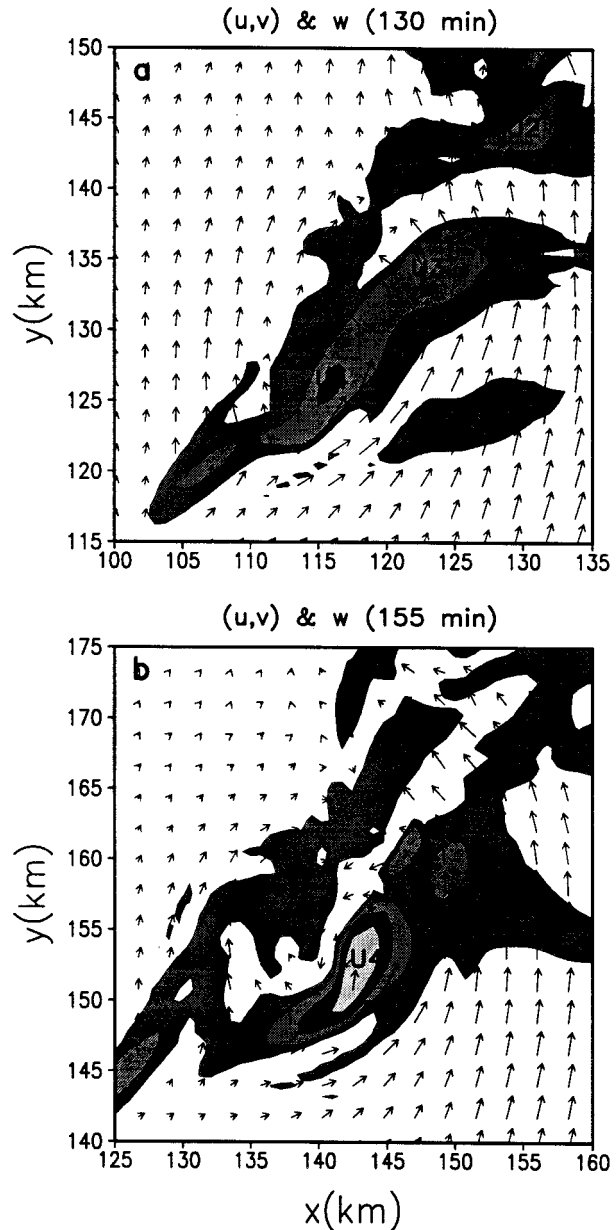


FIG. 10. Same as in Fig. 7 but for (a) 130 and (b) 155 min. The contour levels are shaded at 1, 5, 10, and 15  $m s^{-1}$ .

at about 210 min, and a new updraft forms on its southwest flank. The storm also continues to display HP characteristics, as the updrafts are located within the heavy precipitation mass. The dry slot that first develops in the supercell stage is very pronounced at this time, and a bow echo forms at the tip of the dry slot. The bow echo is best illustrated at higher levels (Fig. 19) and is consistent with one of the life cycles frequently observed in HP supercells (see Fig. 4 in Moller et al. 1994).

The cyclic intensification of the simulated storm is consistent with the evolution of the actual Raleigh tornadic thunderstorm. Three tornadoes were spawned

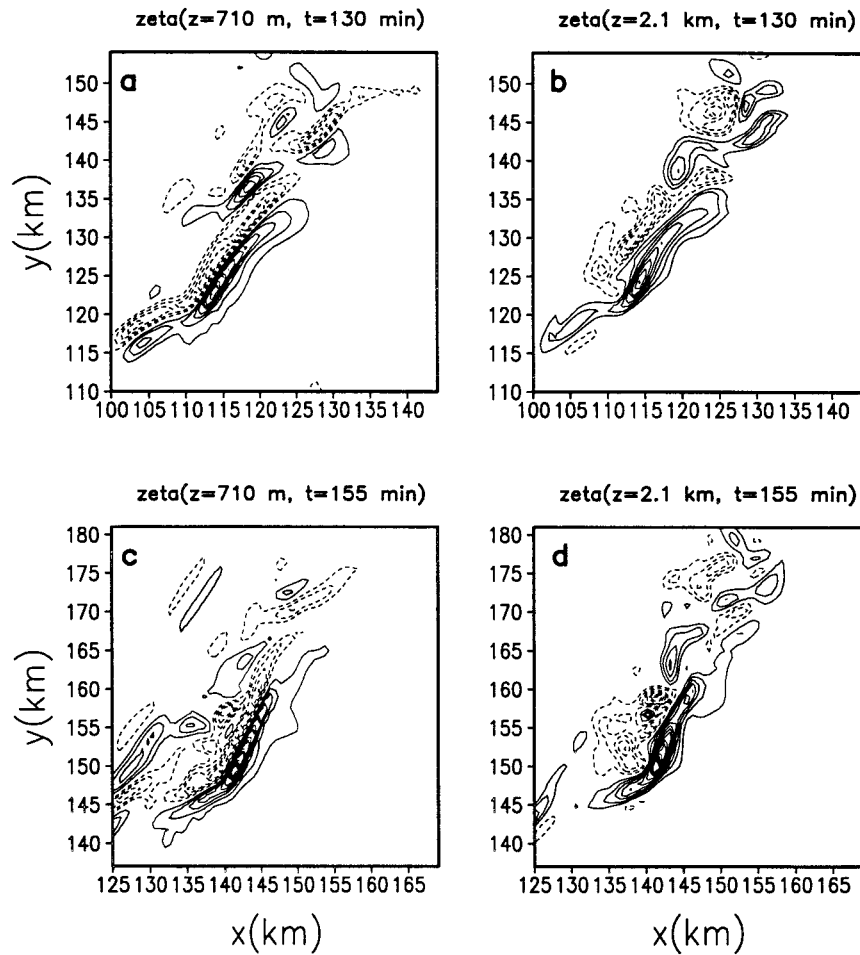


FIG. 11. Same as in Fig. 8 but for (a) and (b) 130 min, and (c) and (d) 155 min.

from the parent thunderstorm throughout its lifetime, indicating that the storm experienced cyclic intensification of low-level vorticity. Whether the tornadoes resulted from the same mesocyclone, or the cyclic production of different mesocyclones, is unknown from the available data. The simulation suggests that cyclic mesocyclogenesis is possible in such a storm, though. The simulated process differs slightly from that proposed by Burgess et al. (1982), in which the occlusion of the gust front is the most important process governing the cyclic growth of mesocyclones within a supercell. No occlusion occurs in the simulation with this grid resolution. Since the updrafts in the reintensification stage are never completely separate entities and actually merge, the new mesocyclone in the simulation may be more accurately described as a reorganization of the old mesocyclone that occurs during this merger process.

#### 4. Updraft structure and intensification mechanisms

A prominent feature of the simulation is the rapid intensification of U4 as the storm evolves from a mul-

ticell to supercell. An intriguing aspect of the storm is the intense low-level updraft core that develops near 165 min that is linked to a pronounced increase in rotation. Such low-level updraft cores have been observed in simulations of hurricane spawned supercells occurring in low-CAPE, strong-shear environments (McCaul and Weisman 1996). The reasons for the updraft structure and intensification in the presently simulated storm, and its implications on vorticity growth, are explored in this section.

Vertical accelerations in convective storms are due primarily to two main factors: buoyancy and vertical pressure gradient effects (Rotunno and Klemp 1985). Prior to the late transition stage, the maximum updrafts in the various cells are located in the upper levels of the storm, corresponding to positive values of buoyancy. This quality further defines the multicell stage, as buoyancy contributions tend to be more important in such storms. As the evolution to a supercell occurs, however, dynamic pressure gradient effects play an increasingly larger role in forcing vertical motions. As seen in Fig. 20, a low perturbation pressure centered near  $z = 2.5$  km occurs between 160 and 170 min. Thus, a large

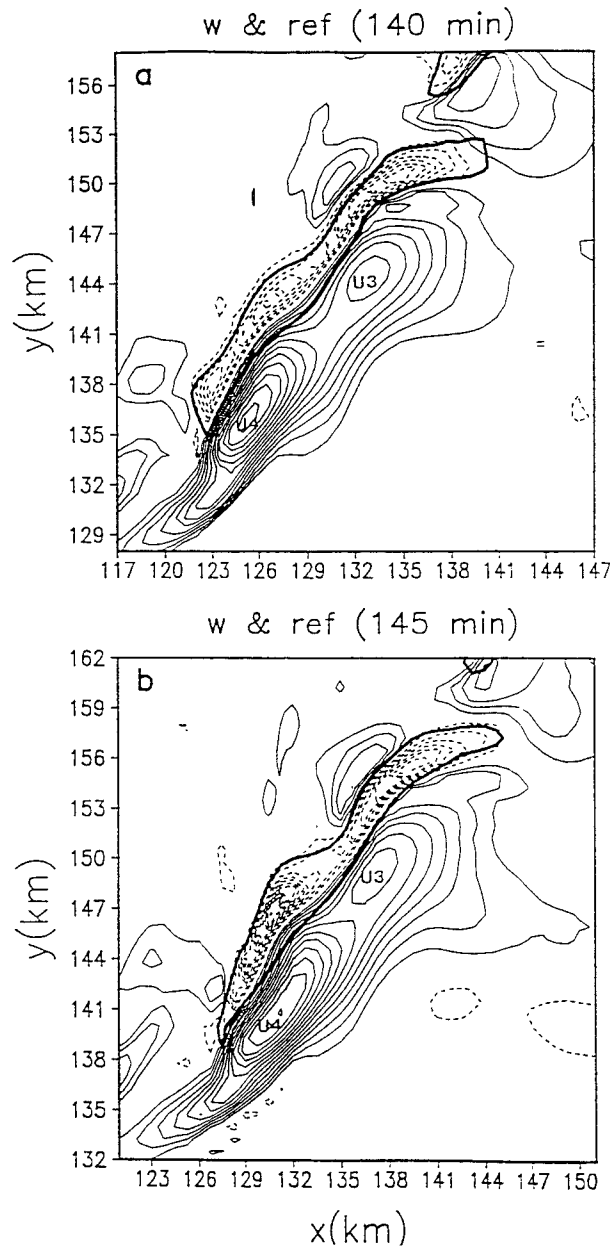


FIG. 12. Vertical velocity at  $z = 1.3$  km for (a) 140 and (b) 145 min. The contour interval is  $1 \text{ m s}^{-1}$ . Positive values are denoted by solid lines, and negative values are denoted by dashed lines. The zero contour is suppressed. The 50-dBZ radar reflectivity contour is superimposed (thick solid contour).

vertical pressure gradient (dynamically induced) exists over the lowest 2.5 km of the storm, and the intense low-level updraft core forms. As  $\partial w/\partial z$  increases, existing vertical vorticity—or vertical vorticity arising from tilted horizontal vortex tubes—is amplified as it undergoes intense stretching.

The exact chain of events that leads to the vorticity increase, low pressure center, and updraft core at low levels is difficult to discern, as changes in the various

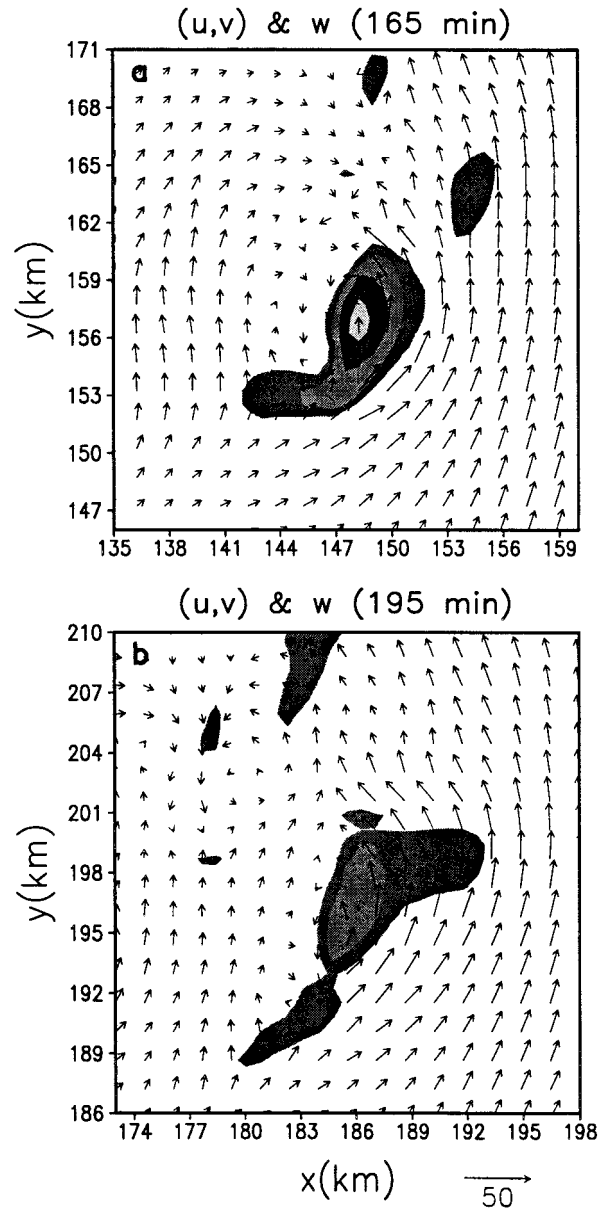


FIG. 13. Same as in Fig. 7 but for (a) 165 and (b) 195 min. The contour levels are shaded at 5, 10, 15, and  $20 \text{ m s}^{-1}$ .

fields often occur almost simultaneously. Careful examination of Figs. 5a and 5b, however, shows that the vertical vorticity is the first field to significantly increase near 125 min, and again after 150 min. A noticeable pressure decrease in the lowest 3 km follows the increase in vorticity at both times. The updraft then strengthens due to favorable pressure gradients as described in the previous paragraph. A fortuitous feedback exists—as the rotation increases between  $z = 1$  and 3 km, the pressure falls, the updraft strengthens, and the change in  $\partial w/\partial z$  becomes very large in the storm's lowest levels. The increase in  $\partial w/\partial z$  then causes increased

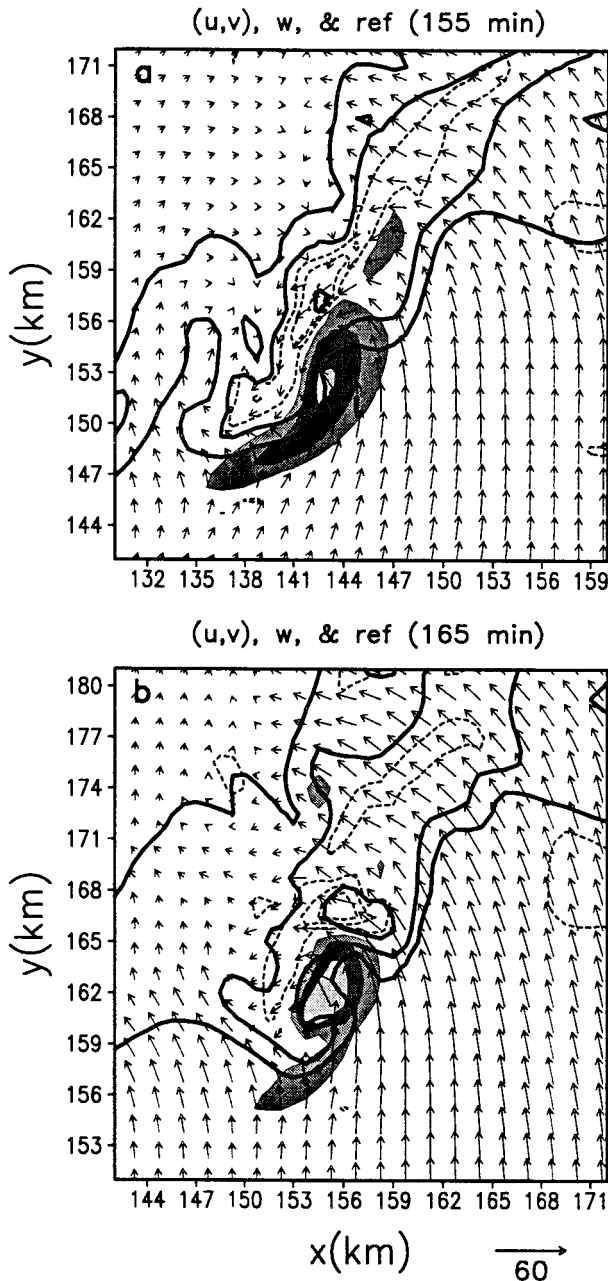


FIG. 14. Storm-relative horizontal wind vectors, vertical velocity, and radar reflectivity at  $z = 1.5$  km for (a) 155 and (b) 165 min. Regions of positive vertical velocity are shaded at 5, 10, and 15  $\text{m s}^{-1}$ . Negative vertical velocity values (dashed) are contoured at  $-1$ ,  $-5$ , and  $-10$   $\text{m s}^{-1}$ . The 30-, 45-, and 60-dBZ reflectivity levels are given by the thick solid lines.

stretching of vorticity, which further enhances the rotation.

McCaul and Weisman (1996) show that the low perturbation pressure in a supercell is often displaced from the main center of vertical vorticity (see their Fig. 5) and is strongly affected by horizontal gyres similar to the one seen in Fig. 17b. Thus, the low perturbation

pressure is still due primarily to dynamic effects, even though it may not be exactly collocated with the center of strongest circulation. McCaul and Weisman also show that dynamic pressure effects are far more important in supercells than buoyancy effects in affecting low-level vertical accelerations. In fact, their landfalling hurricane environment simulation (a similar environment as the present study) produces a supercell with an intense low-level updraft core that is very similar to the present results. The dynamic pressure gradient forcing within this updraft is 3–4 times more important than buoyancy forcing. The emergence of dynamical pressure effects in the present simulation is important in supporting the notion that the simulated storm is indeed supercellular. These dynamic effects in supercells have been well documented and further distinguish supercells from other convective storm types (e.g., Weisman and Klemp 1984; Rotunno and Klemp 1985; Wicker and Wilhelmson 1995; McCaul and Weisman 1996).

Another source of updraft intensification in the simulation results from the merger of various updrafts. This phenomenon is observed throughout the simulation, as updraft maxima merge, resulting in the strengthening and contraction of the updraft. Updrafts forced on the southwest flank of the convective system often merge with the older updraft. The updrafts first separate for a period of time, allowing for the further growth of both updrafts. This separation is followed by an acceleration of the new updraft toward the other, and a merger occurs. The merger process resembles the observations of Lemon (1976), in which the flanking line serves as an intensification source for severe thunderstorms. Updraft perturbations forced along the flanking line were observed to periodically merge with the main system, thus enhancing it. Lemon suggests that the net buoyancy and vertical accelerations in the merged updraft increase via one or more of the following mechanisms: decreased mixing, injection of higher  $\theta$  air, lowering of pressure (and corresponding increase in convergence and rotation) in the mesocyclone, and cloud microphysical effects. Interestingly, the storm complex described by Lemon displays characteristics of a hybrid storm. Therefore, this type of updraft enhancement mechanism seems viable for hybrid multicell–supercell storms that are characterized by multiple updrafts. The environment in which the simulated storm forms seems especially conducive to this process, as there is no convective inhibition and the lifting condensation level is very low. Thus, very little effort is needed to initiate vertical motions, so abundant new updrafts arise that can potentially merge with existing updrafts.

The gust front also plays a vital role in forming and maintaining updrafts throughout the simulation. Forced ascent at the head of the gust front enhances subsequent vertical motions. A well-defined forward gust front develops during the supercell stage that promotes convergence and generates horizontal vorticity that is tilted into the main updraft. It also forces numerous updraft

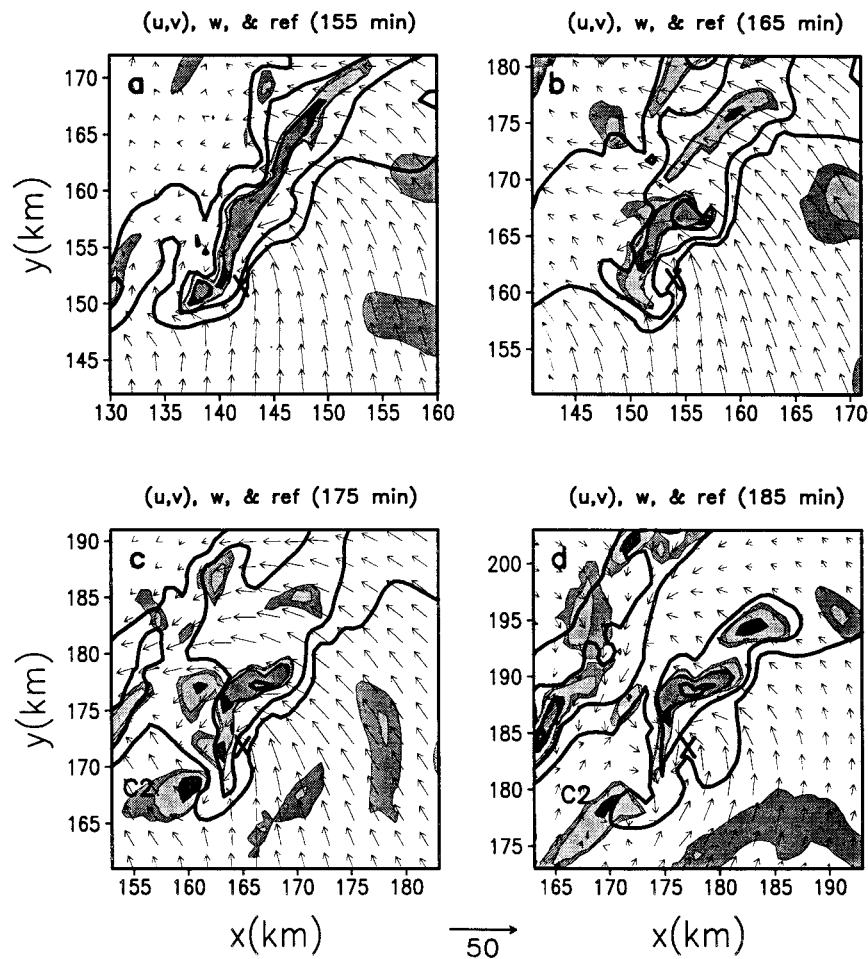


FIG. 15. Storm-relative horizontal wind vectors, downdrafts, and radar reflectivity at  $z = 1.1$  km for (a) 155, (b) 165, (c) 175, and (d) 185 min. Downdrafts are shaded at  $-0.5$ ,  $-1$ ,  $-2$ , and  $-3$   $\text{m s}^{-1}$ . The 30-, 45-, and 60-dBZ reflectivity levels are given by the thick solid lines. The location of U4 at each time is denoted by an "x."

perturbations that are important in the merger process just described. In this simulation, though, the gust front plays a perhaps more important role prior to the supercell stage. Recall that U4 moves along the extensive baroclinic zone that develops from previous cells, thus tapping into the preexisting vertical vorticity, as well as baroclinically generated horizontal vorticity, that is present in this region. The vertical vorticity increases within the updraft, a mesocyclone forms, and the dynamic effects described earlier intensify the updraft and aid in the transformation to a supercellular structure. Without this shallow thermal boundary, the simulated storm may not have acquired the intensity and rotation that it displayed for such a long period of time.

### 5. Vorticity growth

Previous sections have illustrated that the simulated thunderstorm gains intense rotation as it evolves from a multicell- to supercell-type storm. Time-height cross

sections of vertical vorticity also indicate that the vorticity associated with the storm's major updraft originates in the lowest levels of the storm and builds upward (see Fig. 5b). This growth appears to differ from the classic supercell interpretation of vorticity development, in which a midlevel mesocyclone (usually  $\sim 3$ – $6$  km AGL) is first produced by the tilting of environmental horizontal vorticity, and the low-level mesocyclone follows after a baroclinic zone is established near the surface. A representative time-height illustration of this type of vorticity growth can be seen in Fig. 4 of Johnson et al. (1987). In fact, Fig. 5b resembles the development of vorticity associated with nonsupercellular tornadic storms (e.g., Wakimoto and Wilson 1989; Roberts and Wilson 1995; Wakimoto and Atkins 1996). The growth of vorticity in the simulation also seems to fit into the "cool season, strong dynamic HP" category (Przybylinski et al. 1993b). This type of HP storm differs from its warm season counterpart by possessing an often shallow mesocyclone located at lower levels that builds up-

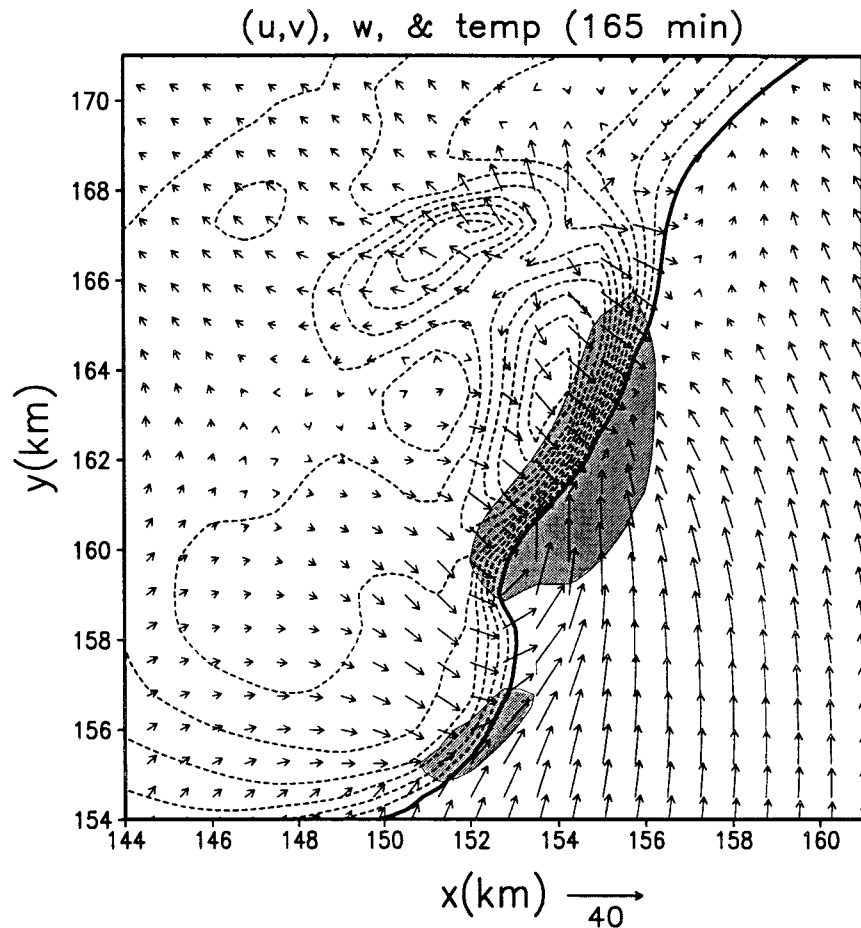


FIG. 16. Ground-relative horizontal wind vectors and negative perturbation temperature (dashed) at  $z = 50$  m for 165 min. The shaded region denotes updrafts of greater than  $3 \text{ m s}^{-1}$  at  $z = 410$  m. The contour interval for the perturbation temperature is  $0.25 \text{ K}$ . The thick solid line denotes the  $0\text{-K}$  contour.

ward. At 165 min, the circulation depth of the simulated mesocyclone is about 5 km, agreeing well with radar observations of cool season HP storms. The circulation center is rather shallow and is located at about  $z = 1.5$  km during the storm's most intense stages.

Figure 21 shows the development of vertical vorticity at various levels for U4 from 65 to 165 min. Significant vertical vorticity exists at  $z = 1.1$  km by 70 min, when U4 is just forming. These values are sustained between  $0.01$  and  $0.011 \text{ s}^{-1}$  until about 110 min, when a steady increase in vorticity occurs. The vorticity increases to over  $0.022 \text{ s}^{-1}$  at 135 min. After 150 min, the vorticity climbs to over  $0.04 \text{ s}^{-1}$  as the storm completes the transition to a supercell. A slight lag exists in the vorticity trends between the various levels. For instance, the vorticity at  $z = 1.1$  km first noticeably rises at 110 min, while the vorticity at  $z = 2.9$  and  $4.5$  km increases at 125 and 135 min, respectively. The vorticity at  $z = 1.1$  km then reaches its peak value at 135 min and is followed by a decrease over the next 10 min. The same trends are observed at  $z = 2.9$  and  $4.5$  km, but they

occur 5 and 10 min later than at  $z = 1.1$  km, respectively. Thus, the rotation originates in the lowest  $\sim 1.5$  km of the storm. Pulses of vorticity from below this level are transported upward over time. This feature is also evident in Fig. 5b, as the phase of the vorticity tilts to the right, signifying upward growth over time.

A closer examination of various terms of the vertical and horizontal vorticity equations sheds additional light on the development of rotation within the main updraft. The generation of vertical vorticity is described by the following equation in Boussinesq form (neglecting turbulent mixing):

$$\frac{D\zeta}{Dt} = \boldsymbol{\eta} \cdot \nabla \mathbf{w} + \zeta \frac{\partial w}{\partial z}, \quad (2)$$

where the first term represents the total derivative of vertical vorticity ( $\zeta$ ), and the second and third terms are tilting of horizontal vorticity ( $\boldsymbol{\eta}$ ) and stretching of vertical vorticity, respectively. The horizontal vorticity equation is

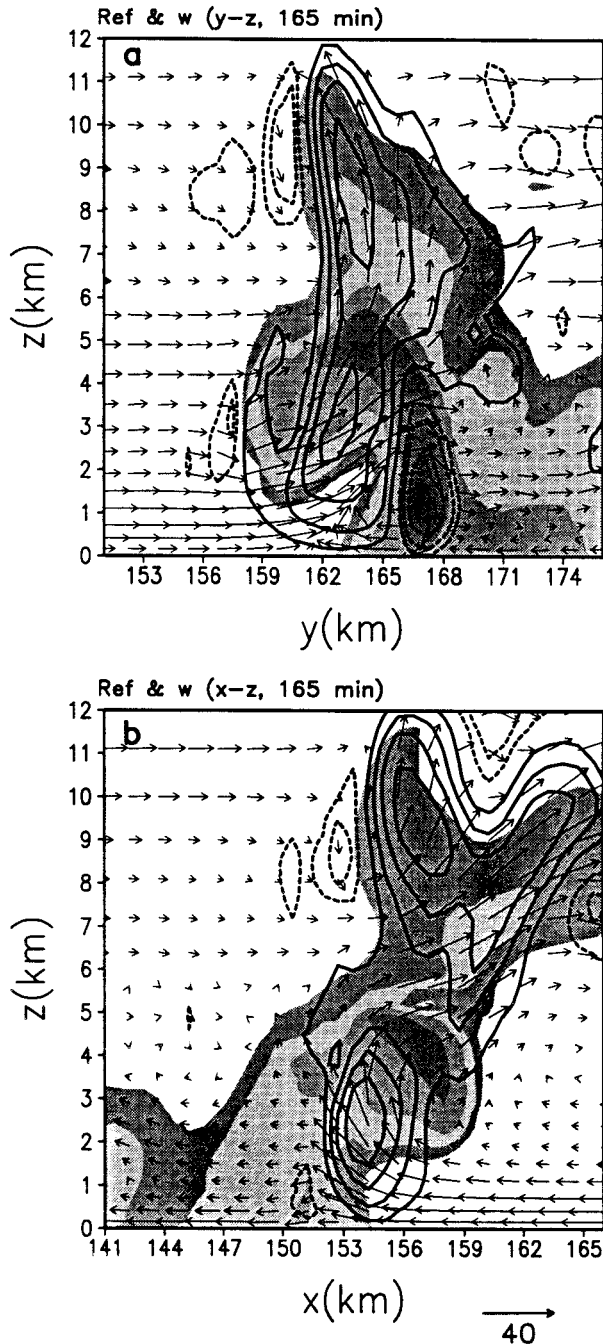


FIG. 17. Cross sections through U4 showing storm-relative wind vectors, radar reflectivity (shaded), and vertical velocity (solid and dashed) at 165 min: (a)  $y$ - $z$  and (b)  $x$ - $z$ . The radar reflectivity levels are shaded from 30 dBZ at 10-dBZ intervals. Positive vertical velocity values (solid lines) are given at 5, 10, 15, and 20  $\text{m s}^{-1}$ . Negative vertical velocity values (dashed lines) are given at  $-2$ ,  $-5$ , and  $-10$   $\text{m s}^{-1}$ . Wind vectors are shown at every other grid point.

$$\frac{D\eta}{Dt} = \boldsymbol{\omega} \cdot \nabla V_h + \nabla \times (B\mathbf{k}), \quad (3)$$

where the terms represent the total derivative of horizontal vorticity, tilting, and solenoidal generation, re-

spectively. The symbols  $\boldsymbol{\omega}$ ,  $\mathbf{V}_h$ , and  $B$  denote the total vorticity vector, the horizontal velocity vector, and the buoyancy, respectively. Figures 22 and 23 depict various terms of the vorticity tendency equations. At 105 min, the production of vertical vorticity is dominated by stretching at  $z = 160$  m (Fig. 22a), while very little tilting (Fig. 22b) occurs near U4. As shown in Fig. 22c, an axis of horizontal vorticity vectors are aligned in a highly streamwise fashion along the buoyancy gradient at 160 m, but no regions of positive tilting exist near U4 to distribute this horizontal vorticity vertically. Even though the buoyancy gradient is not very intense ahead of U4, the baroclinic term in Eq. (3) produces horizontal vorticity at a rate of  $\sim 1.6 \times 10^{-5} \text{ s}^{-2}$  in the lowest 500 m at 105 min. An air parcel that spends 10 min in this baroclinic zone would acquire a horizontal vorticity of near  $0.01 \text{ s}^{-1}$ , so air parcels located along this boundary far ahead of U4 likely have significant horizontal vorticity by the time U4 reaches them. The dominance of vertical vorticity production at 105 min by the stretching of *preexisting* vertical vorticity along the extensive cold pool is also supported by investigating the terms at  $z = 1.1$  km. Stretching is maximized in the vicinity of U4 at this level (Fig. 23a), and little tilting occurs nearby (Fig. 23b).

By 135 min, U4 reaches the most intense section of the thermal boundary. It moves over this boundary for the next 25 min, and a marked increase in vertical vorticity occurs. The stretching term doubles in magnitude at  $z = 160$  m between 105 and 135 min (Fig. 22d), and still exceeds the tilting term (Fig. 22e). Stretching is also the most dominant term in the lowest 1 km of the storm (Fig. 23d). By applying Eq. (2), we see that the convergence term can account for the increase in vertical vorticity. From Fig. 21,  $D\zeta/Dt$  for U4 is  $\sim 1 \times 10^{-5} \text{ s}^{-2}$  at  $z = 1.1$  km from 115 to 135 min. The stretching term produces vertical vorticity at a rate of  $\sim 1 \times 10^{-4} \text{ s}^{-2}$  during the same time period, assuming an average stretching of  $\sim 9 \text{ m s}^{-1}/1100 \text{ m}$  and average  $\zeta$  of  $\sim 0.016 \text{ s}^{-1}$ . Thus, stretching alone can explain the increase in vertical vorticity in U4 from the late multicell to early transition stages. The increase in stretching results from the development of the low-level updraft core, which is its early stages at this time (see Fig. 5a). There is also a small region of low-level positive tilting that forms to the northeast of the vorticity maximum. This coincides with a narrow stream of horizontal vorticity vectors that are parallel to the strengthened buoyancy gradient and storm-relative flow (Fig. 22f). The baroclinic term produces horizontal vorticity at the rate of  $\sim 2.2 \times 10^{-5} \text{ s}^{-2}$  in lower levels at 135 min. Thus, the first signs of positive contributions to the vertical vorticity field from the tilting of baroclinically generated horizontal vorticity are observed near this time. The increase in tilting at  $z = 1.1$  km also reveals the increasingly important role of the tilting of environmental horizontal vorticity as U4 strengthens (Fig. 23e).

Over the next 30 min, U4 evolves into a supercellular

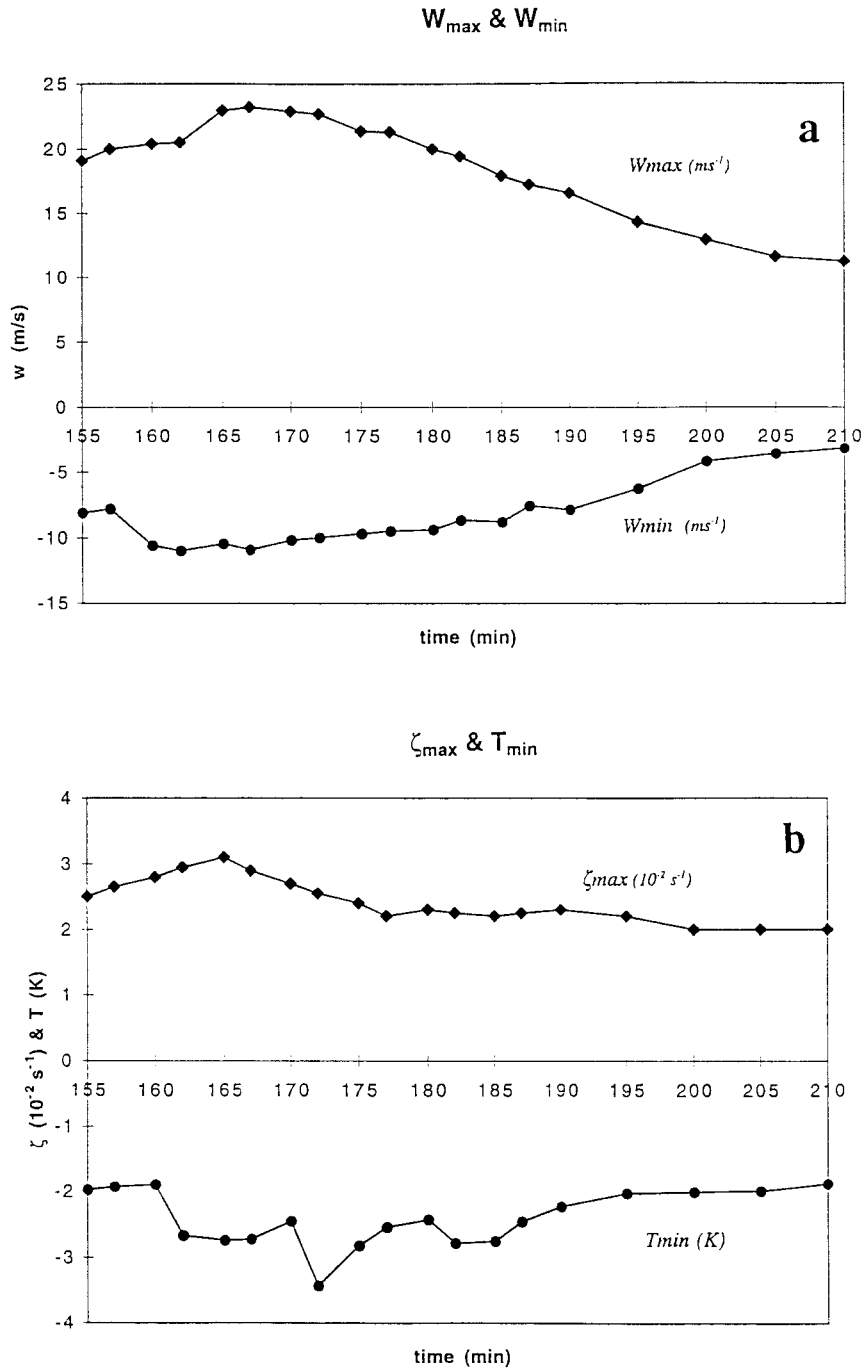


FIG. 18. (a) Maximum vertical velocity (diamonds) and minimum vertical velocity of the FFD (circles) and (b) maximum vertical vorticity (diamonds) and minimum perturbation temperature (circles) of cell U4 from 155 to 210 min. The vertical vorticity values are given in units of  $10^{-2} \text{ s}^{-1}$ . All fields are at  $z = 2.1 \text{ km}$ , except the perturbation temperature, which is at the surface.

structure. The intense low-level updraft core is fully developed by 165 min, and the stretching term almost triples at  $z = 160 \text{ m}$  (Fig. 22g). The stretching term contributes significantly to the generation of vertical vorticity up to almost 2 km, then quickly becomes negligible. The tilting term (Figs. 22h and 23h) also triples

in magnitude, and actually exceeds the stretching term at  $z = 1.5 \text{ km}$ . Even though the magnitude of the tilting term is still much less than the stretching term, tilting is nonetheless important as it becomes a viable source for vertical vorticity that can be amplified by stretching. The horizontal vorticity vectors are also aligned in an

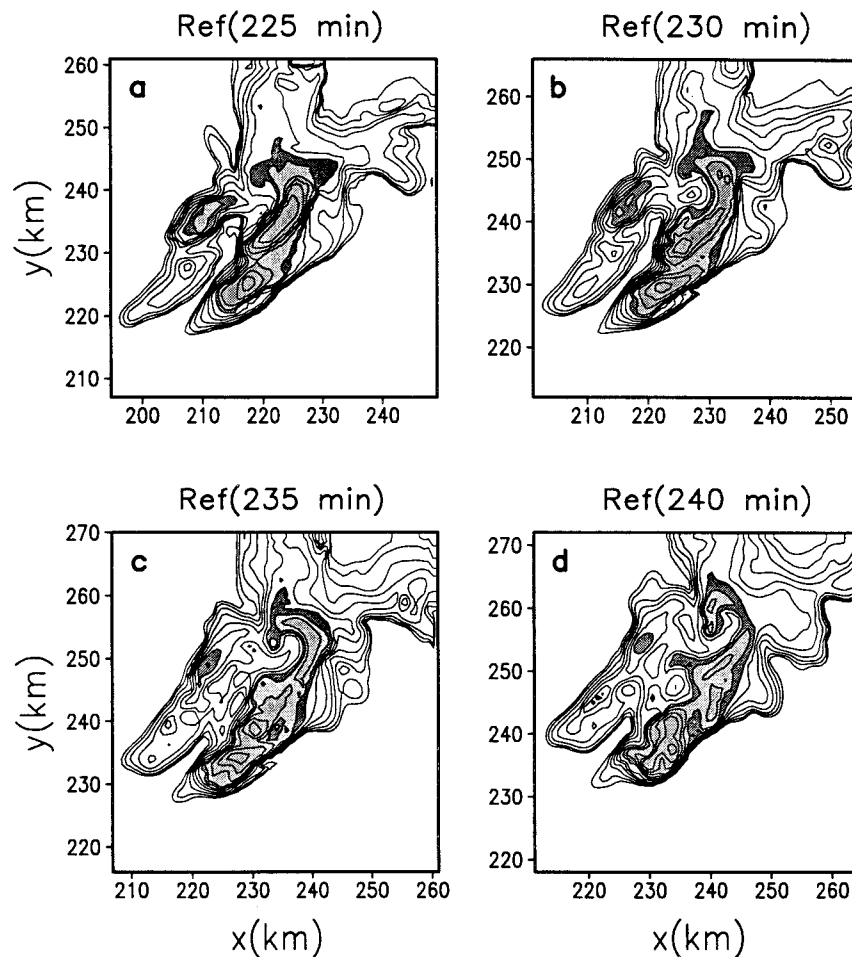


FIG. 19. Same as in Fig. 4 but for (a) 225, (b) 230, (c) 235, and (d) 240 min and  $z = 4.5$  km.

optimal fashion along the intense forward gust front to be ingested by the main updraft (Fig. 23i). *This baroclinic zone, however, is generated directly by the FFD associated with U4, instead of the thermal boundary formed by U2 and U3.* It is much shorter in distance than the preexisting cold pool, and much more vigorous. The baroclinic term reaches its largest magnitude of  $\sim 7 \times 10^{-5} \text{ s}^{-2}$  in the lowest 500 m at this time.

In summary, the simulated storm's main updraft (U4) seems to *initially* acquire its intense rotation via the nonsupercell tornadic storm vorticity generation mechanism of vortex stretching. It should be noted that initial *midlevel* vorticity generation by the same vortex stretching mechanism has been proposed for supercell storms (e.g., Brown 1992). However, the source of the ambient vertical vorticity in Brown's study is different than the current simulation results, as it was due to a midlevel positive vorticity region on the downwind flank of a nonrotating updraft. This vorticity was then entrained and stretched by a different updraft that developed on the right flank of the original updraft. As U4 strengthens, vorticity production is aided by contributions from the

tilting of both environmentally and baroclinically generated horizontal vorticity—mechanisms associated more with supercell storms. Thus, the storm evolves into a supercellular structure in a slightly different manner than the “traditional” isolated classic supercell. Classic supercell mechanisms are working, however, throughout the simulation and are indeed very important. For instance, a left-moving, anticyclonically rotating cell produced by the storm-splitting process was observed early in the simulation. Also, the vorticity-rich environment that U4 encounters can be directly attributed to the production of two previous mesocyclones (U2 and U3). These mesocyclones formed by the more conventional supercell method of the tilting of environmental horizontal vortex tubes (see Fig. 8), but they did not mature into intensely rotating cells like U4. Perhaps the strongly sheared environment inhibited these updrafts from gaining a strong supercellular appearance, yet they enabled the subsequent development of U4 by altering the initial environment to make it more conducive to a stronger, longer lasting mesocyclone later in the simulation. This shielding effect, along with the

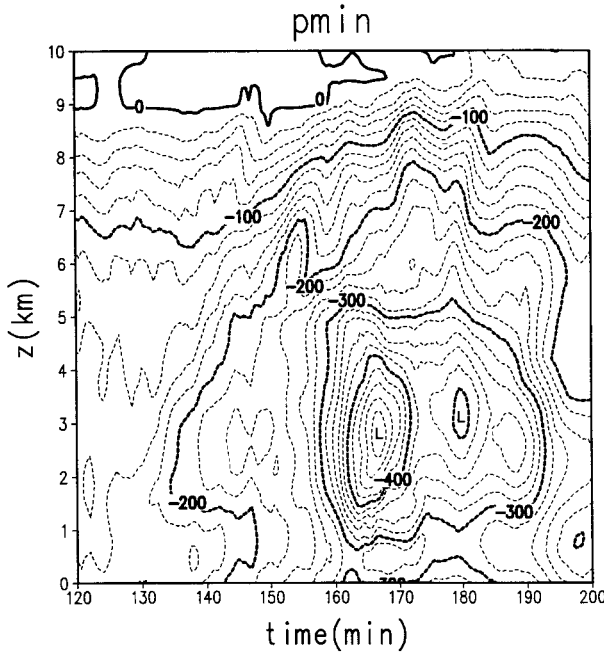


FIG. 20. Time–height cross section of domain minimum perturbation pressure from 120 to 200 min. The contour interval is 20 Pa.

storm-scale interactions described earlier (i.e., tapping into the preexisting vertical vorticity and horizontal vorticity within the cold pool) allows U4 to evolve into an intense supercell. Since the structure and evolution of simulated storm closely resembles the observed Raleigh

tornadic thunderstorm, similar localized shielding effects and storm-scale interactions could play an important role in the acquisition of rotation in multiple-updraft convective storms that form in similar cold season, strong dynamic environments.

**6. Summary and conclusions**

A cloud-scale numerical model (TASS) is employed to study the structure and evolution of a multiple-updraft, HP supercell complex. The model is initialized with a sounding taken from a mesoscale modeling study of the 28 November 1988 Raleigh tornadic thunderstorm. Major findings of the simulation include the following.

- TASS produces a convective storm that compares favorably with many of the observed features of the actual Raleigh tornadic thunderstorm.
- The simulated storm possesses structural features of hybrid multicell–supercell storms (e.g., Foote and Frank 1983; Nelson 1987), as well as HP supercells.
- The simulated storm undergoes a transition from a multicell storm to a multiple-updraft supercell storm with intense storm-scale rotation. Interactions between the cells of the convective complex are important during this transition, as an updraft strengthens and acquires significant rotation as it moves along a boundary created by older cells. Both the stretching of preexisting vertical vorticity (due to tilted environmental horizontal vorticity by previous updrafts)

**Domain Maximum Vertical Vorticity**

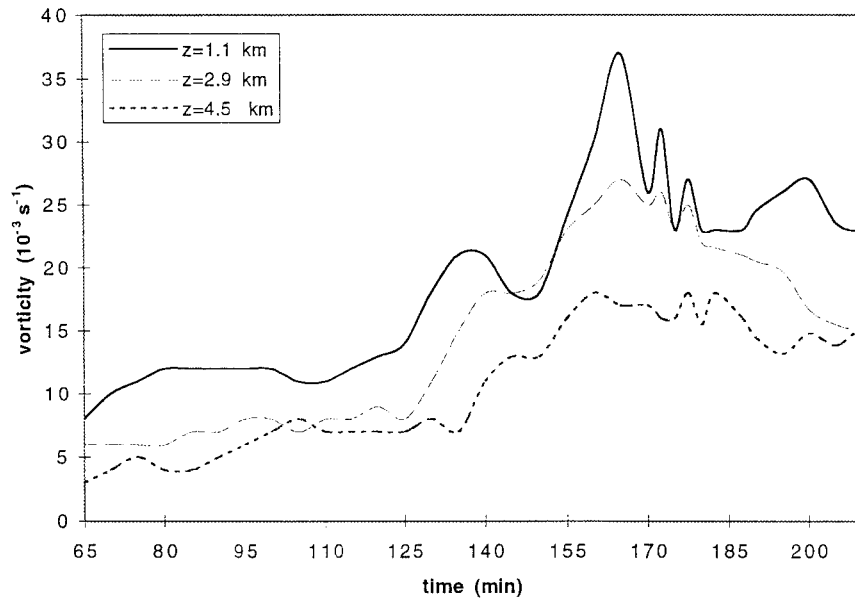


FIG. 21. Maximum vertical vorticity associated with U4 at  $z = 1.1, 2.9,$  and  $4.4$  km from 65 to 210 min.

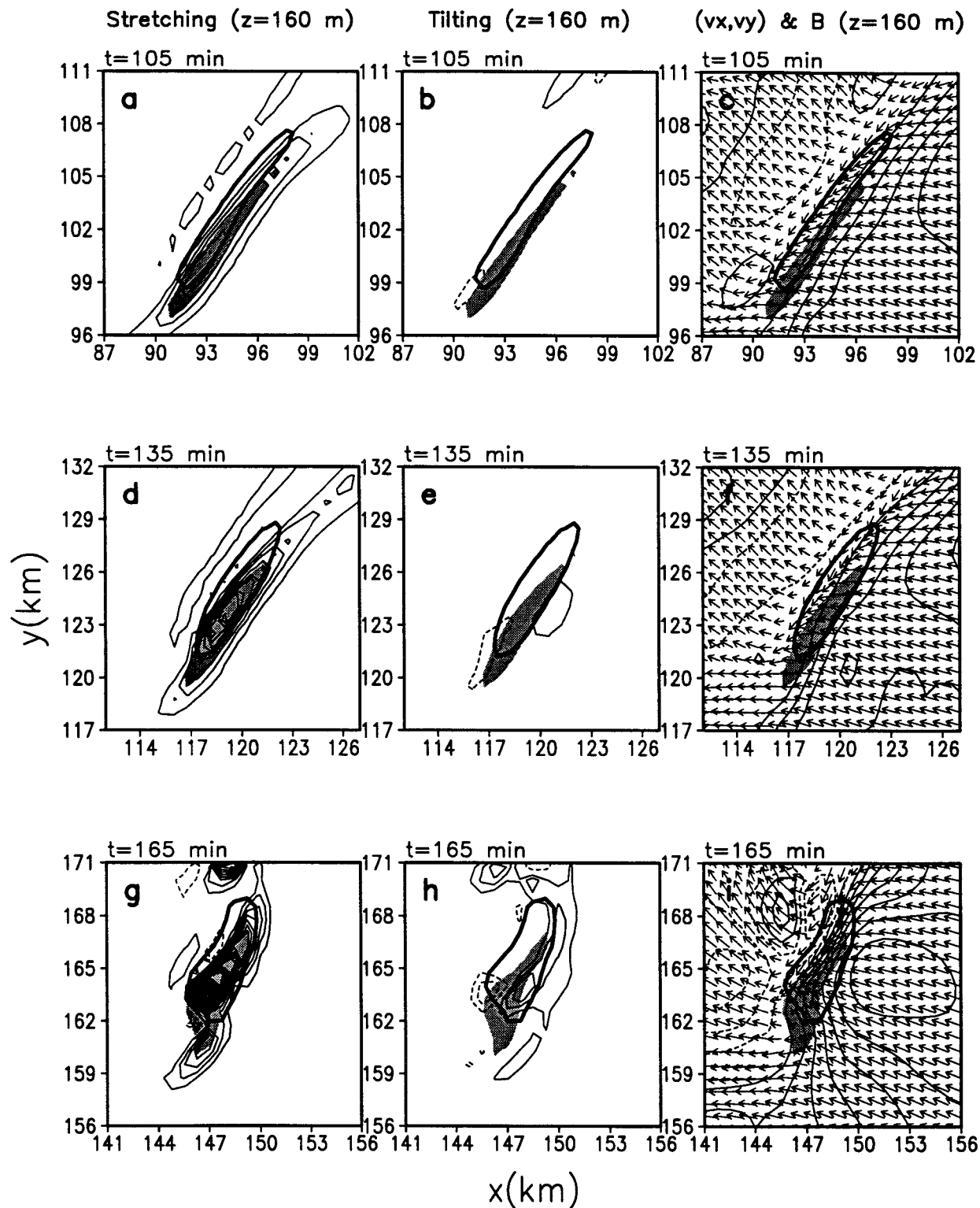


FIG. 22. Contributions to vorticity production from the terms in Eqs. (2) and (3) at  $z = 160$  m. Vertical vorticity production due to stretching at 105, 135, and 165 min is shown in (a), (d), and (g), respectively. Vertical vorticity production due to tilting at 105, 135, and 165 min is shown in (b), (e), and (h), respectively. The horizontal vorticity vectors and buoyancy field at 105, 135, and 165 min are shown in (c), (f), and (i), respectively. Regions of vertical vorticity  $> 0.01 \text{ s}^{-1}$  at  $z = 160$  m (shaded) and  $z = 1.5$  km (thick solid line) are also shown. The contour intervals for the stretching, tilting, and buoyancy fields are  $2 \times 10^{-5} \text{ s}^{-2}$ ,  $2 \times 10^{-5} \text{ s}^{-2}$ , and  $0.01 \text{ m s}^{-2}$ , respectively.

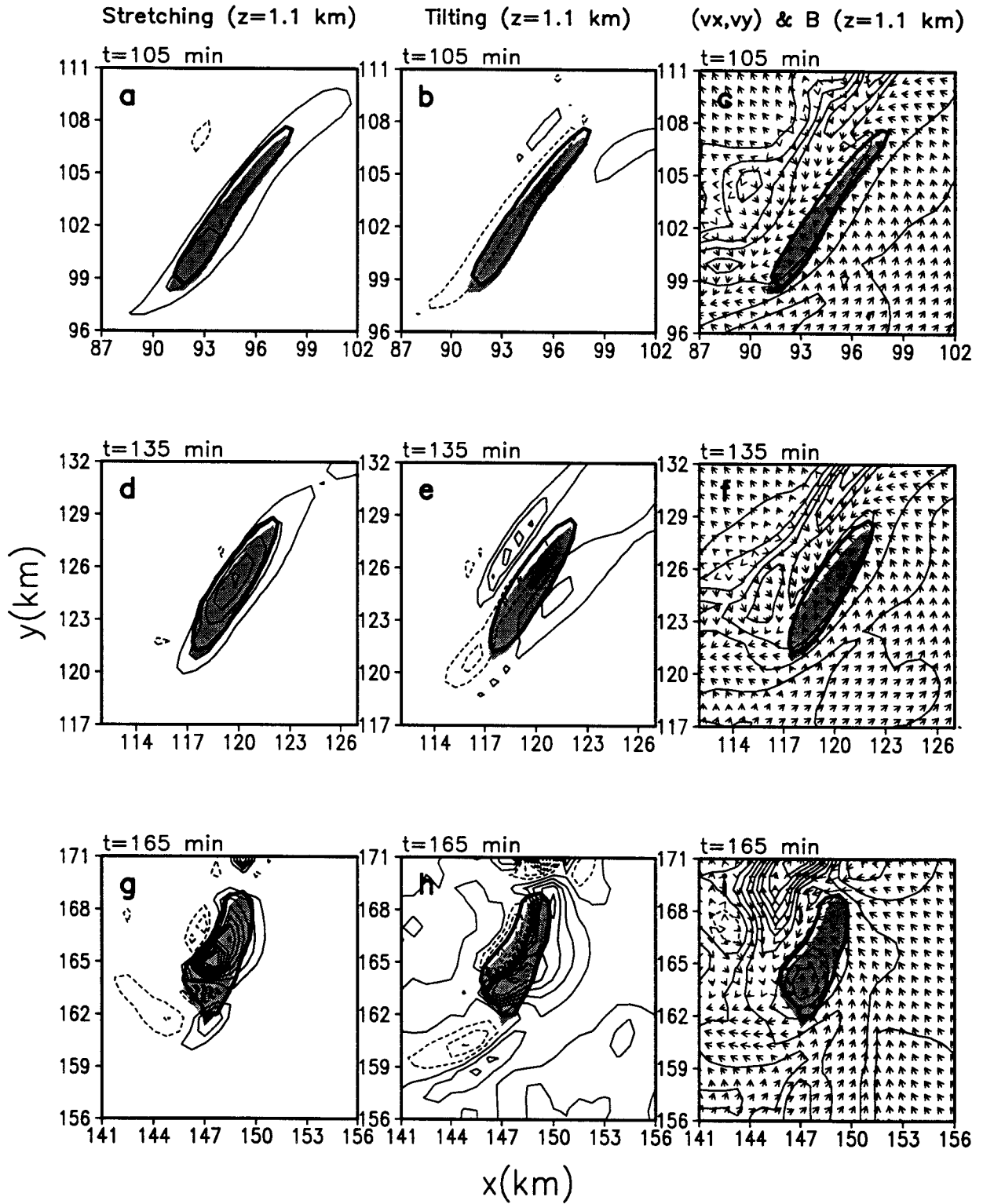


FIG. 23. Same as in Fig. 22 but for  $z = 1.1$  km.

and the tilting of baroclinically generated horizontal vorticity along the boundary are important in producing vertical vorticity in the storm's transition to a supercell.

- The intensity of the mature storm is maintained despite displaying HP supercell characteristics. Pulsating rear flank downdrafts, as well as updraft mergers, are hypothesized to play a vital role in maintaining storm-scale rotation and updraft intensity. Also, the rear gust front never occludes in the mature storm, possibly due to the dominance of the low-level shear compared to the strength of the cold pool.
- The development of vorticity conforms to conceptual models of cool season, strong dynamic HP storms (Przybylinski et al. 1993b). Significant vertical vorticity in the main updraft originates in the lowest portions of the storm and builds upward over time, similar in appearance to nonsupercellular tornadic storms. However, the significance of the tilting and stretching of baroclinically generated and environmental *horizontal* vorticity as the storm matures better fits the supercell development of vertical vorticity. This model of vorticity development seems most applicable to thunderstorm complexes that have interacting cells, or individual thunderstorms that encounter shallow mesoscale thermal boundaries.

An obvious disadvantage of these modeling results is the constraint of a horizontally homogeneous basic state and the inclusion of a rather unnatural method of initialization. A cloud-scale model that incorporates the fine mesoscale subtleties that existed in the dynamic environment that produced the Raleigh tornado would provide interesting results to compare with the present study. Also, the ability to nest down to a finer scale to observe whether (and how) tornadogenesis occurs in the simulation would be very useful. Additional simulations to test the storm's sensitivity to sounding and microphysical characteristics, as well as a rigorous trajectory analysis, would also yield beneficial results to build upon the present findings. Despite these deficiencies, the simulation results presented in this study offer further insight to the structural and evolutionary complexity of certain supercell thunderstorms. It also provides a unique opportunity to investigate HP supercell development in a cold season, strong dynamic environment that does not conform exactly to classical models.

*Acknowledgments.* This work is supported by NSF Grant ATM-9224595 and NOAA Grant NA27RP029201. The comments of Dr. Michael Kaplan, Dr. Steven Koch, Mr. Roy Deal, Mr. David DeCroix, Mr. Robert Rozumalski, Mr. Ron Przybylinski, and two anonymous reviewers are greatly appreciated. We also gratefully acknowledge Dr. Fred Proctor for his input and for providing the numerical model (TASS) used in this study. Thanks also to Dr. John Zack for supplying the sounding used to initialize TASS. Computations were performed

on IBM work stations, which are part of the FOAM<sup>v</sup> computing facility at NCSU, and the supercomputer at the North Carolina Supercomputing Center.

#### REFERENCES

- Bluestein, H. B., and C. R. Parks, 1983: A synoptic and photographic climatology of 786 low-precipitation severe thunderstorms in the southern plains. *Mon. Wea. Rev.*, **111**, 2034–2046.
- Brady, R. H., and E. Szoke, 1989: A case study of nonmesocyclone tornado development in northeast Colorado: Similarities to waterspout formation. *Mon. Wea. Rev.*, **117**, 843–856.
- Brooks, H. E., C. A. Doswell III, and R. B. Wilhelmson, 1994: The role of midtropospheric winds in the evolution and maintenance of low-level mesocyclones. *Mon. Wea. Rev.*, **122**, 126–136.
- Brown, R. A., 1992: Initiation and evolution of updraft rotation within an incipient supercell thunderstorm. *J. Atmos. Sci.*, **49**, 1997–2014.
- Browning, P. A., J. E. Hales Jr., and L. F. Wilson, 1989: Factors contributing to the Raleigh tornado of 28 November 1988. Preprints, *12th Conf. on Weather Analysis and Forecasting*, Monterey, CA, Amer. Meteor. Soc., 167–172.
- Burgess, D. W., V. T. Wood, and R. A. Brown, 1982: Mesocyclone evolution statistics. Preprints, *12th Conf. on Severe Local Storms*, San Antonio, TX, Amer. Meteor. Soc., 422–424.
- Carbone, R. E., 1983: A severe frontal rainband. Part II: Tornado parent vortex circulation. *J. Atmos. Sci.*, **40**, 2639–2654.
- Davies-Jones, R. P., 1984: Streamwise vorticity: The origin of updraft rotation in supercell storms. *J. Atmos. Sci.*, **41**, 2991–3006.
- , D. Burgess, and M. Foster, 1990: Test of helicity as a tornado forecast parameter. Preprints, *16th Conf. on Severe Local Storms*, Kananaskis Park, AB, Canada, Amer. Meteor. Soc., 588–592.
- Doswell, C. A., III, A. R. Moller, and R. W. Przybylinski, 1990: A unified set of conceptual models for variations on the supercell theme. Preprints, *16th Conf. on Severe Local Storms*, Kananaskis Park, AB, Canada, Amer. Meteor. Soc., 40–45.
- Foote, G. B., and H. W. Frank, 1983: Case study of a hailstorm in Colorado. Part III: Airflow from triple-Doppler measurements. *J. Atmos. Sci.*, **40**, 686–707.
- Funk, S., 1991: An analysis of the tornado-producing Raleigh thunderstorm of November 28, 1988. M.S. thesis, Dept. of Marine, Earth, and Atmospheric Sciences, North Carolina State University, 98 pp. [Available from Dept. of Marine, Earth, and Atmospheric Sciences, North Carolina State University, Raleigh, NC 27695.]
- Gonski, R. F., B. P. Woods, and W. D. Korotky, 1989: The Raleigh tornado—28 November 1988: An operational perspective. Preprints, *12th Conf. on Weather Analysis and Forecasting*, Monterey, CA, Amer. Meteor. Soc., 173–178.
- Johns, R. H., J. M. Davies, and P. W. Leftwich, 1993: Some wind and instability parameters associated with strong and violent tornadoes. Part II: Variations in the combinations of wind and instability parameters. *The Tornado: Its Structure, Dynamics, Prediction and Hazards, Geophys. Monogr.*, No. 79, Amer. Geophys. Union, 583–590.
- Johnson, K. W., P. S. Ray, B. C. Johnson, and R. P. Davies-Jones, 1987: Observations related to the rotational dynamics of the 20 May 1977 tornadic storms. *Mon. Wea. Rev.*, **115**, 2463–2478.
- Kaplan, M. L., R. A. Rozumalski, R. P. Weglarz, Y.-L. Lin, S. Businger, and R. F. Gonski, 1995: Numerical simulation studies of the mesoscale environment conducive to the Raleigh tornado. NOAA Tech. Memo. NWS ER-90, 101 pp. [Available from Y.-L. Lin, Dept. of Marine, Earth, and Atmospheric Sciences, North Carolina State University, Raleigh, NC 27695-8208.]
- Klemp, J. B., and R. B. Wilhelmson, 1978: Simulations of right- and left-moving storms produced through storm splitting. *J. Atmos. Sci.*, **35**, 1097–1110.
- , and R. Rotunno, 1983: A study of the tornadic region within a supercell thunderstorm. *J. Atmos. Sci.*, **40**, 359–377.

- , R. B. Wilhelmson, and P. S. Ray, 1981: Observed and numerically simulated structure of a mature supercell thunderstorm. *J. Atmos. Sci.*, **38**, 1558–1580.
- Korotky, W. D., 1990: The Raleigh tornado of November 28, 1988: The evolution of a tornadic environment. Preprints, *16th Conf. on Severe Local Storms*, Kananaskis Park, AB, Canada, Amer. Meteor. Soc., 532–537.
- Lemon, L. R., 1976: The flanking line, a severe thunderstorm intensification source. *J. Atmos. Sci.*, **33**, 686–694.
- , and C. A. Doswell III, 1979: Severe thunderstorm evolution and mesocyclone structure as related to tornadogenesis. *Mon. Wea. Rev.*, **107**, 1184–1197.
- Lin, Y.-L., R. D. Farley, and H. D. Orville, 1983: Bulk parameterization of the snow field in a cloud model. *J. Climate Appl. Meteor.*, **22**, 1065–1092.
- Maddox, R. A., L. R. Hoxit, and C. F. Chappell, 1980: A study of tornadic thunderstorm interactions with thermal boundaries. *Mon. Wea. Rev.*, **108**, 322–336.
- Marwitz, J. D., 1972: The structure and motion of severe hailstorms. Part 2: Multicell storms. *J. Appl. Meteor.*, **11**, 180–188.
- McCaul, E. W., and M. L. Weisman, 1996: Simulations of shallow supercell storms in landfalling hurricane environments. *Mon. Wea. Rev.*, **124**, 408–429.
- MESO, 1993: MASS version 5.5 reference manual. MESO, Inc., 118 pp.
- Mogil, H. M., and G. P. Ellrod, 1989: The Raleigh tornado of November 28, 1988: Interpreting satellite signatures. Preprints, *12th Conf. on Weather Analysis and Forecasting*, Monterey, CA, Amer. Meteor. Soc., 179–185.
- Moller, A. R., C. A. Doswell III, M. P. Foster, and G. R. Woodall, 1994: The operational recognition of supercell thunderstorm environments and storm structures. *Wea. Forecasting*, **9**, 327–347.
- Monin, A. S., and A. M. Obukhov, 1954: Basic laws of turbulent mixing in the atmosphere near the ground. *Tr. Geofiz. Inst., Akad. Nauk., SSSR*, **151**, 1963–1987.
- Nelson, S. P., 1987: The hybrid multicellular-supercellular storm—An efficient hail producer. Part II: General characteristics and implications for hail growth. *J. Atmos. Sci.*, **44**, 2060–2073.
- NOAA, 1988: *Storm Data*. Vol. 11, NOAA, 72 pp.
- Orlanski, I., 1976: A simple boundary condition for unbounded hyperbolic flows. *J. Comput. Phys.*, **21**, 251–269.
- Proctor, F. H., 1987: The Terminal Area Simulation System. Vol. I, Theoretical formulation. NASA Contractor Rep. 4046, NASA, Washington, DC, 176 pp. [Available from Y.-L. Lin, Dept. of Marine, Earth, and Atmospheric Sciences, North Carolina State University, Raleigh, NC 27695-8208.]
- , 1989: Numerical simulations of an isolated microburst. Part II: Sensitivity experiments. *J. Atmos. Sci.*, **46**, 2143–2165.
- , 1992: Three-dimensional simulation of the Denver 11 July 1988 microburst-producing storm. *Meteor. Atmos. Phys.*, **49**, 107–124.
- , 1996: Numerical simulation of wake vortices measured during the Idaho Falls and Memphis Field Programs. AIAA Paper No. 96-2496, 18 pp. [Available from NASA, Washington, DC.]
- Przybylinski, R. W., 1989: The Raleigh tornado—28 November 1988: A radar overview. Preprints, *12th Conf. on Weather Analysis and Forecasting*, Monterey, CA, Amer. Meteor. Soc., 186–191.
- , S. Runnels, P. Spoden, and S. Summy, 1990: The Allendale, Illinois, tornado—January 7, 1989. One type of an HP supercell. Preprints, *16th Conf. on Severe Local Storms*, Kananaskis Park, AB, Canada, Amer. Meteor. Soc., 516–521.
- , J. T. Snow, E. M. Agee, and J. T. Curran, 1993a: The use of volumetric radar data to identify supercells: A case study of June 2, 1990. *The Tornado: Its Structure, Dynamics, Prediction and Hazards*, *Geophys. Monogr.*, No. 79, Amer. Geophys. Union, 241–250.
- , T. J. Shea, D. L. Ferry, E. H. Goetsch, R. R. Czys, and N. E. Wescott, 1993b: Doppler radar observations of high-precipitation supercells over the mid-Mississippi Valley region. Preprints, *17th Conf. on Severe Local Storms*, St. Louis, MO, Amer. Meteor. Soc., 158–163.
- Purdom, J. F. W., 1993: Satellite observations of tornadic thunderstorms. *The Tornado: Its Structure, Dynamics, Prediction and Hazards*, *Geophys. Monogr.*, No. 79, Amer. Geophys. Union, 265–274.
- Roberts, R. D., and J. W. Wilson, 1995: The genesis of three non-supercell tornadoes observed with dual-Doppler radar. *Mon. Wea. Rev.*, **123**, 3408–3436.
- Rotunno, R., and J. B. Klemp, 1985: On the rotation and propagation of simulated supercell thunderstorms. *J. Atmos. Sci.*, **42**, 271–292.
- , —, and M. L. Weisman, 1988: A theory for strong, long-lived squall lines. *J. Atmos. Sci.*, **45**, 463–485.
- Smagorinsky, J., 1963: General circulation experiments with the primitive equations. Part I: The basic experiment. *Mon. Wea. Rev.*, **91**, 99–164.
- Vasiloff, S. V., E. A. Brandes, R. P. Davies-Jones, and P. S. Ray, 1986: An investigation of the transition from multicell to supercell storms. *J. Climate Appl. Meteor.*, **25**, 1022–1036.
- Wakimoto, R. M., and J. W. Wilson, 1989: Non-supercell tornadoes. *Mon. Wea. Rev.*, **117**, 1113–1140.
- , and N. T. Atkins, 1996: Observations on the origin of rotation: The Newcastle tornado during VORTEX 94. *Mon. Wea. Rev.*, **124**, 384–407.
- Weaver, J. F., and S. P. Nelson, 1982: Multiscale aspects of thunderstorm gust fronts and their effects on subsequent storm development. *Mon. Wea. Rev.*, **110**, 707–718.
- Weisman, M. L., and J. B. Klemp, 1984: The structure and classification of numerically simulated convective storms in directionally varying wind shears. *Mon. Wea. Rev.*, **112**, 2479–2498.
- Wicker, L. J., and R. B. Wilhelmson, 1995: Simulation and analysis of tornado development and decay within a three-dimensional supercell thunderstorm. *J. Atmos. Sci.*, **52**, 2675–2703.
- Zack, J. W., P. E. Price, K. T. Waight, and M. D. Bousquet, 1993: Numerical simulation and analysis of cold-season severe weather events. Final Rep. to the Dept. of Commerce, NOAA Contract No. 50-DKNA-2-00120, 131 pp. [Available from Y.-L. Lin, Dept. of Marine, Earth, and Atmospheric Sciences, North Carolina State University, Raleigh, NC 27695-8208.]
- , —, —, and —, 1994: A numerical-dynamical investigation of the rapid mesoscale evolution associated with the Raleigh, North Carolina, tornado event of November 28, 1988. Preprints, *Sixth Conf. on Mesoscale Processes*, Portland, OR, Amer. Meteor. Soc., 138–139.